CO₂ and hydrography acquired by Autonomous Surface Vehicles from the Atlantic Ocean to the Mediterranean Sea: data correction and validation

Riccardo Martellucci[1], Michele Giani[1], Elena Mauri[1], Laurent Coppola[2], Melf Paulsen[3], Marine Fourrier[2], Sara Pensieri[4], Vanessa Cardin[1], Carlotta Dentico[5], Roberto Bozzano[4], Carolina Cantoni[6], Anna Luchetta[6], Alfredo Izquierdo[7], Miguel Bruno[7], and Ingunn Skjelvan[8]

[1]National Institute of Oceanography and Applied Geophysics (OGS), Trieste, Italy

[2]Oceanography Laboratory of Villefranche (LOV), Villefranche, France

[3]GEOMAR Helmholtz Centre for Ocean Research Kiel, Kiel, Germany

[4]National Research Council - Institute for the study of Anthropic Impact and Sustainability in the Marine Environment (CNR-IAS), Genova, Italy

[5]Department of Environmental Sciences, Informatics and Statistics, Università Cà Foscari, Venice,, Italy

[6]National Research Council-Institute of Marine Sciences (CNR-ISMAR), Trieste, Italy

[7]University of Cádiz (UCA), Spain

[8]NORCE Norwegian Research Centre, Bjerknes Centre for Climate Research. Beregn, Norway

Corresponding author: Riccardo Martellucci (rmartellucci@ogs.it)

Abstract. The ATL2MED demonstration experiment involved two autonomous surface vehicles from Saildrone Inc. (SD) which travelled a route from the eastern tropical North Atlantic to the Adriatic Sea between October 2019 and July 2020. This nine-month experiment in a transition zone between the temperate and tropical belts represents a major challenge for SD's operations. The sensors on board were exposed to varying degrees of degradation and biofouling depending on the geographical area and season, which led to a deterioration of the measurements. As a result, some maintenance measures were required during the mission.

We address the difficulty of correcting the data during a period of COVID-19 restrictions, which significantly reduced the number of discrete samples planned for SD salinity and dissolved oxygen validation. This article details alternative correction methods for salinity and dissolved oxygen. Due to the lack of *in situ* data, model products have been used to correct the salinity data acquired by the SDs, and then the resulting corrected salinity was validated with data from fixed ocean stations, gliders, and Argo floats. In addition, dissolved oxygen data acquired from SDs after correction using air oxygen measurements were tested and found to be coherent with the variation of oxygen concentrations expected from change in temperature and phytoplankton abundance (from chlorophyll-a). The correction methods are relevant and useful in situations where validation capabilities are lacking, which was the case during the ATL2MED demonstration experiment. For future experiments, a more frequent sample collection would improve the data qualification and validation.

1 Introduction

Automated observations contribute to a steadily increasing knowledge of the ocean and its role in the global climate system. For a long time, fixed ocean stations and research vessels formed the backbone of the monitoring network. In recent years, efforts have been made to improve the frequency of acquisition through technological developments (*e.g.*, EU infrastructures ICOS, https://www.icos-cp.eu/; EMSO, https://emso.eu; EuroArgo,

41 https://www.euro-argo.eu). Among other improvements, fixed ocean stations and ships of opportunity (Lüger et
42 al., 2004) were equipped with autonomous and accurate sensors for partial pressure of CO_2 (pCO_2) measurements
43 in addition to sensors for complementary measurements (*e.g.*, water temperature, salinity, dissolved oxygen, pH,
44 nutrients, fluorescence) needed to understand the dynamics and the effects of CO_2 fluxes on the carbon budget.
45 Despite efforts to do so, it remains difficult to obtain a comprehensive overview of CO_2 fluxes at regional and
46 larger scales because of very sparse coverage by fixed observatories, low measurement frequency and limited
47 systematic reference measurements.

48 One way to address such observational gaps (Tanhua et al., 2019) is to develop and deploy Autonomous Surface
49 Vehicles (ASV) equipped with a suite of sensors, and capable of measuring CO_2 fluxes at the air-sea interface with
50 gas reference, high sampling frequency and real-time data transmission. ASV monitoring systems have the
51 potential to collect data from large ocean areas and at a frequency that resolves processes at multiple time scales.
52 Nevertheless, there are challenges with those surface monitoring systems, and one of the most important is
53 biofouling, which can interfere with measurements of *e.g.*, conductivity, dissolved oxygen and especially
54 chlorophyll-a (Chl-a), and could ultimately render the sensors inoperable (*e.g.*, Delauney et al., 2010). Regular
55 maintenance counteracts biofouling or at least reduces the impact on measurements, but this is not always possible
56 due to long distance from shore or from the maintenance vessel. Therefore, the value of ASV data depends heavily
57 on quality control and quality assurance.

58 During the 9-month-long demonstration experiment ATL2MED, two wind-driven Saildrone ASV (SD;
59 Gentemann et al., 2020) manufactured by Saildrone Inc. (Alameda, CA, USA) were used to improve data coverage
60 and link CO_2 surface observations at fixed ocean stations on a larger scale from the eastern tropical North Atlantic
61 (ETNA) to the central Mediterranean Sea. SDs are prone to errors primarily due to sensor drift, which can be
62 caused by either biofouling or malfunctioning sensor parts. During the ATL2MED demonstration experiment,
63 problems were found with the data collected by several SD sensors, and severe biofouling occurred, as expected
64 in such a long-duration experiment.

65 Still, the use of SDs provided the opportunity to expand and link fixed CO_2 observations at the surface on a
66 larger scale, particularly during the COVID-19 pandemic when access to ocean platforms and ship visits were
67 restricted or even prohibited. Furthermore, the demonstration experiment allowed us to focus SD measurements
68 on different marine environments, the Atlantic Ocean and the Mediterranean Sea, which made it possible to assess
69 the quality of measurements across a wide range of values. The experiment additionally evaluated the ability of
70 such ASV to provide data with sufficient quality to be relevant for the scientific community.

71 The objective of the present work is to evaluate and correct the data collected by the SDs in order to provide
72 a homogenised and comparable data set useful for the study of processes such as air-sea gas exchange in the
73 Atlantic Ocean and Mediterranean Sea. While this paper focuses on the methods, a follow up paper will focus on
74 biogeochemical processes occurring in the area.

75

2 Material

2.1 Data collection and experiment

78 The ATL2MED demonstration experiment took place between 18 October 2019 and 17 July 2020 as a joint effort
79 among a number of European academic institutions and SD piloting team. A detailed description of the ATL2MED
80 demonstration experiment can be found in Skjelvan et al. (2021). During the experiment, the SDs crossed the
81 ETNA region, the Strait of Gibraltar, and the northern part of the western and central Mediterranean Sea including
82 the Ligurian Sea, the Strait of Sicily, the Strait of Otranto, and the Adriatic Sea (Fig. 1).

83 The aim of the ATL2MED demonstration experiment was to (1) study eddies in the Canary Current upwelling
84 system off West Africa jointly with a vessel-based research expedition (RV Meteor M160) and (2) to validate the
85 CO_2 measurements acquired at 5 fixed ocean stations (DYFAMED, W1M3A, E2M3A, PALOMA, and
86 MIRAMARE). This monitoring experiment was achieved with sensors and instruments installed on the SDs, but
87 also equipment deployed at a number of facilities that were used to correct data from the SDs (see Section 3).
88 Table 1 provides an overview of the various facilities and the times at which the SD visits were carried out. A
89 detailed description of the instruments and sensors installed on the different platforms as well as their
90 characteristics can be found in Tables S1, S2 and S3 of the Supplementary Material.

Figure 1. Study area, with the upper map showing the route of the two SDs (SD 1030 black and SD 1053 red lines), the positions of the Argo floats (yellow dots) and the SD routes divided into transects (T). The lower maps zoom in on areas with in-situ observations (buoys, ships and glider sections).
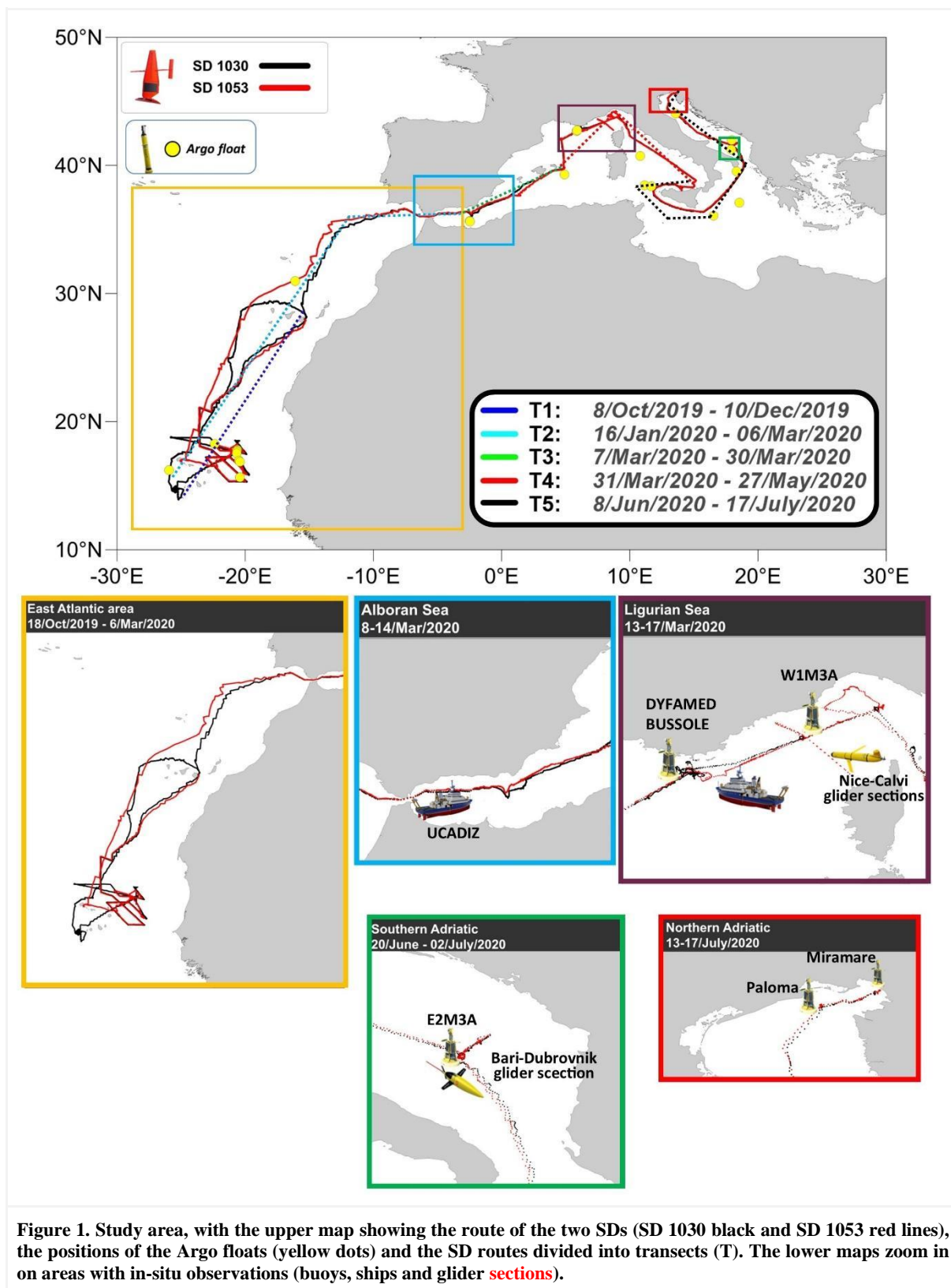
91

92 Maintenance operations ensured the reliability and accuracy of the data collected by the SDs. Throughout the
93 expedition, the data collected by the SDs were categorised into different transects, designated as T1, T2, T3, T4,
94 and T5. These transects corresponded to specific sections of the expedition timeline in terms of maintenance events
95 (see Table S1 in Supplementary Material), which facilitates data correction.

96   The SDs were equipped with a number of autonomous sensors (CTD: conductivity, temperature, depth;
97   dissolved oxygen; fluorescence; pH; pCO$_2$; meteorological sensors). This study focuses primarily on sensors
98   acquiring temperature, salinity, dissolved oxygen, and pCO$_2$ data. This selection is based on the available options
99   for correcting the SD datasets: some of the sensors (*e.g.*, fluorescence) were so severely affected by biofouling
100   that it could not be accounted for, while others only worked for a short period of time (*e.g.*, Durafet Honeywell
101   pH sensor). One of the SDs (SD 1030) was equipped with an ASVCO2 system developed by PMEL (NOAA's
102   Pacific Marine Environmental Laboratory). The ASVCO2 system is a compressed version of the more voluminous
103   system described in detail in Sutton et al. (2014) and Sabine et al. (2020). Water from a depth of approximately
104   0.5 m is fed into a bubble equilibrator (Friederich et al., 1995) and the partially dried xCO$_2$ is measured with an
105   infrared detector (LI-COR 820 CO2 gas analyser). A two points calibration was used where the first is a reference
106   gas from NOAA/ERSL, while the second is air purged for CO$_2$. An air inlet was mounted approximately 1 m
107   above sea level and atmospheric xCO$_2$ was measured between measurements of the sea surface. See Table S2 in
108   the Supplementary Material for the measurement frequency and initial accuracy of the SD sensors during the
109   ATL2MED experiment.

110

2.2 Comparative datasets

2.2.1 Liguro-Provencal basin facilities

113   In the French EEZ, the open-ocean station DYFAMED is located in the Ligurian Sea in the northwestern
114   Mediterranean Sea. The CNRS (French National Centre for Scientific Research) is in charge of the station as part
115   of the national MOOSE program (Coppola et al., 2019). At the DYFAMED site, a CARIOCA pCO$_2$ sensor ensures
116   autonomous measurements and detailed description can be found in Merlivat et al. (2018). In addition, gliders are
117   regularly operating the Nice-Calvi section where the DYFAMED site is located (MOOSE program; Coppola et
118   al., 2019; Bosse et al., 2015; Testor et al., 2019). During the demonstration experiment, a deployment of the
119   Slocum glider was used along the endurance line (MOOSE T00-43 mission) performed from 12 March to 20 June
120   2020. Table S2 includes information about which sensors the glider was equipped with. Discrete samples were
121   collected from the DYFAMED site in February and March 2020 for comparison with the pCO$_2$ sensor
122   measurements (Table S4).
123   The open-ocean station W1M3A is located in the Italian EEZ of the Liguro-Provencal basin. Operated by
124   CNR-IAS, the W1M3A consists of a large spar buoy and a subsurface mooring positioned in the immediate
125   vicinity. A detailed description of the observatory can be found in Canepa et al. (2015) and some of this information
126   is found in Table S2. Discrete samples were collected from W1M3A in October 2020 (Table S4).

127

2.2.2   Adriatic Sea facilities

129   The fixed station E2M3A is situated in the open sea of the southern Adriatic Sea and is operated by Italian National
130   Institute of Oceanography and Applied Geophysics - OGS. Information on this site is found in Bozzano et al.
131   (2013) and Ravaioli et al. (2016). In the southern Adriatic, OGS also regularly operates an ocean glider at the Bari-
132   Dubrovnik section (Mauri et al., 2016; Pirro et al., 2022; Kokkini et al., 2019). During the ATL2MED
133   demonstration experiment, the glider transect was extended to include the area of the E2M3A fixed station from
134   12 June to 2 July 2020. During the 20-day campaign 250 dives between 20 to 950 m profiles separated by 3-5 km
135   and 4-6 hours were collected. Table S2 contains information about the specific sensors mounted at the glider.
136   In the Gulf of Trieste in the northern Adriatic, the coastal stations PALOMA (operated by CNR-ISMAR) and
137   MIRAMARE (operated by OGS) are situated. Description of the PALOMA station is found in Ravaioli et al.
138   (2016) and Cantoni et al. (2012), while the MIRAMARE site is described in Ravaioli et al. (2016). See Table S2
139   for information about which sensors are used at the sites. By means of comparing the pCO$_2$ sensor measurements
140   performed at the sites, discrete carbon samples were collected near PALOMA on 15 July 2020 and in the vicinity
141   of MIRAMARE on 17 July 2020 (Table S4).

142

143 **2.3 Shipboard data**

144 Discrete samples for Dissolved Inorganic Carbon (DIC) and TA were collected onboard the RV Meteor (M160)
145 during fall 2019 and analysed by GEOMAR. Discrete samples for DIC, TA, pH, and dissolved oxygen are
146 regularly collected next to the fixed ocean stations, however, this was not always possible during the ATL2MED
147 demonstration experiment due to COVID-19 pandemic restrictions. Table S4 gives an overview of the discrete
148 samples collected during the ATL2MED demonstration experiment and their sampling depth and analysing
149 methods.
150   In addition, salinity was measured continuously on board of the RV Ucadiz at a depth of 2.3 m between 5 and
151 6 March 2020, when the SD crossed the Gibraltar Strait. Table S2 contains information about the sensor used.

152
153 **Table 1. Research vessels and fixed ocean stations from which temperature, salinity and/or carbon measurements were**
154 **compared with those of the SDs.**

Research vessel/ fixed station	Position	Institution	SD 1030	SD 1053
RV Meteor	17.80°N 20.60°W	GEOMAR (DE)	30 November 2019	12 December 2019
RV Ucadiz	36.55°N 6.31°W - 36.09°N 5.36°W	UCA (ES)	5-6 March 2020	5-6 March 2020
DYFAMED	43.42°N 7.87°E	CNRS (FR)	28 April 2020	23 April 2020
W1M3A*	43.83°N 9.12°E	CNR-IAS (IT)	29 April-2 May 2020	28 April-2 May 2020
E2M3A*	41.57°N 18.08°E	OGS (IT)	29 June-2 July 2020	29 June-23 July 2020
PALOMA*	45.62°N 13.57°E	CNR-ISMAR (IT)	15 July 2020	15 July 2020
MIRAMARE*	45.70°N 13.71°E	OGS (IT)	17 July 2020	17 July 2020

155 * These stations are part of the ICOS station network (Steinhoff et al., 2019).
156

157 **2.4 Argo Float**

158 Float data were retrieved from the Argo Coriolis Global Data Assembly Center in France (GDAC;
159 ftp://ftp.ifremer.fr/argo, Wong et al., 2020). For each Argo float the variable SALINITY_ADJUSTED was
160 extracted, and then used for comparison with SD salinity data. Every profile close in space and time (1 day and 30
161 km) was chosen and then salinity was averaged in the upper 5 m of the water column.
162

163 **2.5 Model output**

164 The Copernicus Marine Service (CMEMS) model product, specifically the Global Ocean 1/12° Physics Analysis
165 and Forecast (https://doi.org/10.48670/moi-00016) and the Mediterranean Sea Physics Analysis and Forecast
166 (Escudier et al,. 2020, Clementi et al., 2021) were used. Daily data were developed for the global ocean and
167 Mediterranean Sea.
168

169 **2.6 Satellite product**

170 To evaluate the ocean response, sea surface Chl-a (OCEANCOLOUR_MED_BGC_L3_NRT_009_141), sea
171 surface temperature (Merchant et al., 2019, Buongiorno Nardelli er al., 2022) and the vertical structure of ocean

172   temperature (MEDSEA_MULTIYEAR_PHY_006_004) were downloaded from the CMEMS data portal and
173   analysed (Table S6 in the Supplementary Material).

174

3 Methods

3.1 Salinity

177   Here, the salinity is measured using the PSS-78 scale. During the first transect, T1 (Fig. 2), the two salinity sensors
178   on board the SDs showed high consistency (Fig. 2a, b). After the first maintenance in T2, the SD 1053 showed a
179   reduction in salinity of about 1 compared to the salinity measured by the SD 1030. In T3, the difference in salinity
180   decreased on average to 0.15. During this period, the SDs crossed the Alboran Sea characterised by high
181   thermohaline variability due to the presence of Atlantic and Mediterranean waters (Poulain et al., 2021), and the
182   high spatial and temporal variability in salinity distribution in the area (Capó et al., 2021) complicates the
183   understanding of the observed differences (i.e., sensor error or natural variability). In T4 and T5, salinity shifts of
184   1 were observed until the end of the experiment.

185   Given the large variability found in the salinity data of the SDs, a comparison with *in situ* data along the
186   trajectory of the experiment was necessary. We first identified the observing systems (fixed buoy, Argo float)
187   temporally and spatially close to the positions of the SDs. Salinity data, with a temporal and spatial interval lower
188   than 1 day and 30 km, respectively, were used for the comparison and/or correlation, however they were extremely
189   scarce.

190   To further evaluate the salinity data of the two SDs, a comparison was made with climatological data,
191   considering the closest point in the climatology dataset to the SDs measurements (Fig. 2). SD 1030 exhibited
192   consistent salinity data in periods T1, T2, and T4 (ΔS <0.1), with deviations observed in periods T3 and T5 (Fig.
193   2a). Conversely, SD 1053 displayed consistent salinity data only in period T1 (ΔS <0.1), with higher deviations in
194   periods T2, T3, T4, and T5. Subsequent evaluation of the data distribution characteristics revealed variances
195   between the two SDs (Fig. 2b).

196   In T5, the climatology failed to represent salinity in Ionian and Adriatic Sea, characterised by a continuous
197   increase in salinity since 2017 (Mauri et al., 2021; Mihanović et al., 2021; Menna et al., 2022; Neri et al., 2023;
198   Pranic et al., 2023). This was due to the bipolar behaviour of the Ionian Sea, subject to an alternation between the
199   highly saline waters of the Levantine Basin and the less saline waters of Atlantic origin (Pinardi et al., 2019; Gačić
200   et al., 2021; Menna et al., 2022; Civitarese et al., 2023).

201   To overcome the problem of lack of data, we decided to compare the data acquired by the SDs with the
202   reanalysis model products along the entire route (Fig. 2a, b). The model, while not deviating much from the *in situ*
203   and climatological data (Fig. 2), can provide salinity products along the SD's trajectory allowing for the correction
204   of the salinity recorded by the SD. Moreover, comparative works between the physical model and experimental
205   observations have shown a satisfactory correlation both in the open ocean (Escudier et al., 2021; Menna et al.,
206   2023) and in the coastal environment (Martellucci et al., 2021). Despite all the limitations a model may have in
207   such cases, the use of model products allows a minimum spatial and temporal distance in the comparison of the
208   along track SD measurements. The nearest nodes (in km) with respect to the model data grid to the SD trajectory
209   were chosen. The salinity provided by the model along the two SD trajectories shows very similar values to that
210   measured by SD 1030 (Fig. 3). Salinity differences between the CMEMS model and the SD 1030 observations
211   show a difference less than 0.1 in T1, T2, T4 and T5. During the Alboran Sea crossing (T3), the observed salinity
212   deviated strongly from the model (about 0.6) over only 20 days. In contrast, SD 1053 showed deviating values
213   compared to the model and SD 1030, which cannot be explained by space-time variability. With the exception of
214   T1, the remaining transects (Fig. 3i-j) showed large deviations between model and observed salinities (T2: 0.8,
215   T3: 0.7, T4: 0.9, and T5: 1). This could be related to the long time between the SD 1053 maintenance (early January
216   and early May 2020), but it is more likely that a sensor error occurred in mid-January which even maintenance
217   could not correct.

218   The salinity correction was performed using a linear regression method in which the salinity data recorded by
219   the autonomous vehicles averaged over the day, were calibrated with the corresponding data from numerical
220   models. A strict criterion, with a significance level of $p < 0.05$ (Table 2), was applied to the correction process.

221

Figure 2. Salinity time series of daily raw data, CMEMS model salinity products, climatology and float data. (a) SD 1030 salinity raw data (black line), model (dotted blue line) and climatological (green circle) data from nearest nodes to the SD trajectory, and *in situ* data (yellow diamonds). (b) SD 1053 salinity raw data (red line), CMEMS model 1053 trajectory (dotted cyan line), climatological data (green circle) and *in situ* platforms (yellow diamonds). Numbers close to diamonds indicate the distance (km) from the trajectory of SD. *In situ* platforms include data from Argo buoys, fixed stations, gliders and RV Ucadiz.

222

223 **Table 2. Statistics for the salinity correction. T1, to T5 refer to the different transects, pval is the significance level,**
224 **distribution refers to normal or non normal data distribution, R^2 is the correlation coefficient, RMSE is the root mean**
225 **square error, and NaN refers to lack of data.**

		Direct comparison				
		T1	*T2*	*T3*	*T4*	*T5*
SD 1030	*pval*	0.0007	0.04	<0.001	0.04	0.025
	distribution	non normal	non normal	normal	non normal	normal
	R2	0.59	0.61	0.19	0.71	0.85
	RMSE	-	-	0.9058	-	0.2789

SD 1053	pval	0.026	0.003	0.004	<0.001	<0.001
	distribution	non normal	normal	normal	normal	normal
	R2	0.08	0.44	0.25	0.789	0.919
	RMSE	-	0.826	0.7072	0.8444	1.1275

226

227

Figure 3. Least square regression between model and SD raw salinity during each transect from T1 (left) to T5 (right) for SD 1030 (a, b, c, d, e) and SD 1053 (f, g, h, i, j). The solid line represents the linear regression fit.

228
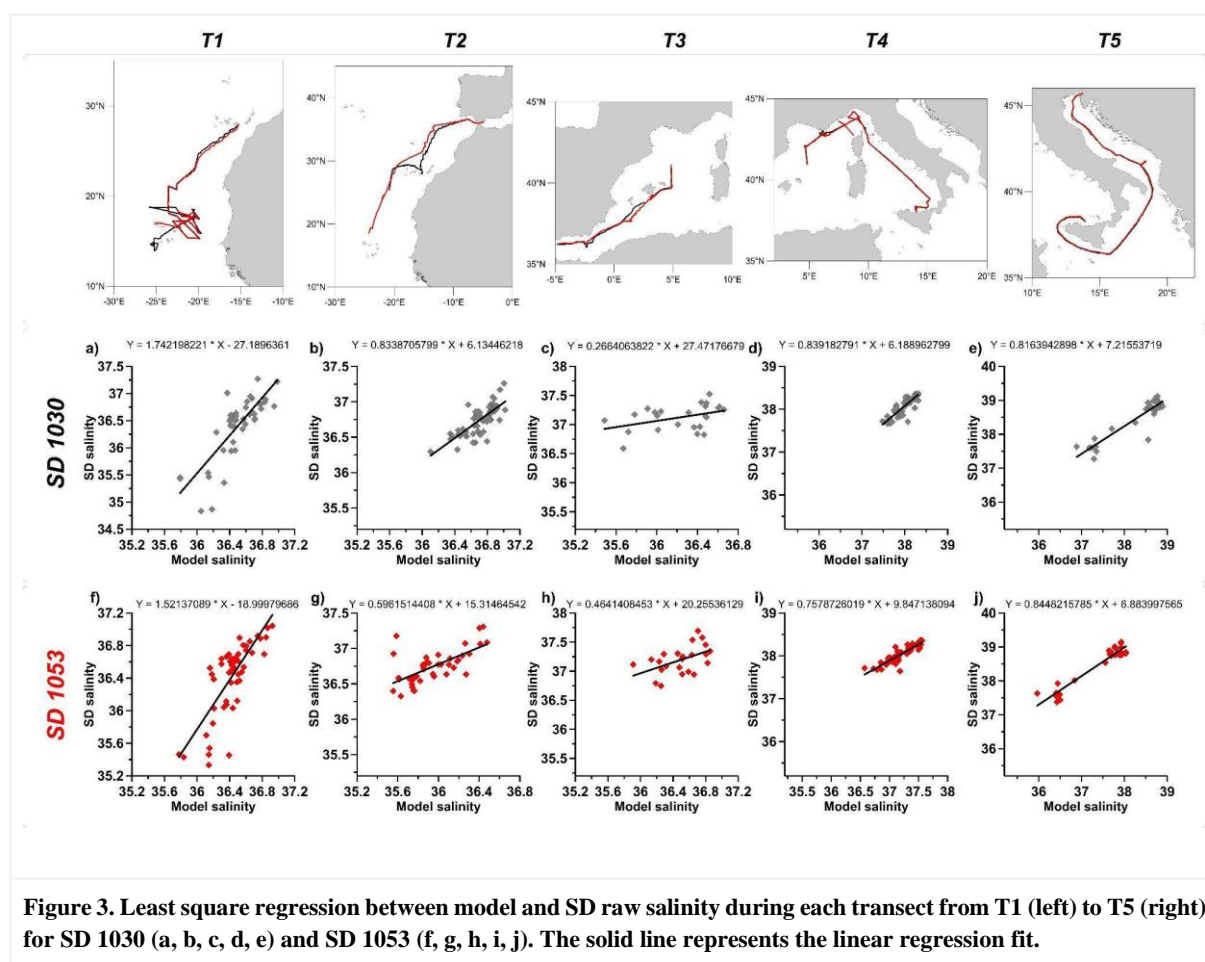
3.2 Dissolved Oxygen

230 Due to the strong dependence of dissolved oxygen on temperature, we first analyse the temperature along the track
231 of the SDs. During the demonstration experiment, sea temperature (Fig. 4a) showed a seasonal signal similar to
232 those observed at these latitudes (Pastor et al., 2019). The high observed temperature variability also includes the
233 wide geographical coverage of the SDs. The highest temperatures were measured in November 2019 and July
234 2020 in the tropical Atlantic and the southern Adriatic, respectively. The lowest temperatures were measured in
235 the Gulf of Lion in April 2020. Along the SD tracks, the salinity (Fig. 2b) showed a gradual increase from the
236 Atlantic Ocean to the eastern Mediterranean Sea. Given the correct temperature measurement, any dissolved
237 oxygen drift can be assessed through comparison with dissolved oxygen saturation values. This procedure was

also used to correct Argo float data with climatological observations (Takeshita et al., 2013). The dissolved oxygen
saturation showed a gradual decrease from 100% at the start of the demonstration experiment to 80% at the end
(Fig. 4c). This behaviour is also reflected in the dissolved oxygen concentration, which decreases by about 40
μmol/kg for SD 1030 and 60 μmol/kg for SD 1053 (Fig. 4b) over the course of nine months with standard deviation
of the uncorrected oxygen record of 16 μmol/kg and 72 μmol/kg for SDs 1030 and 1053, respectively.
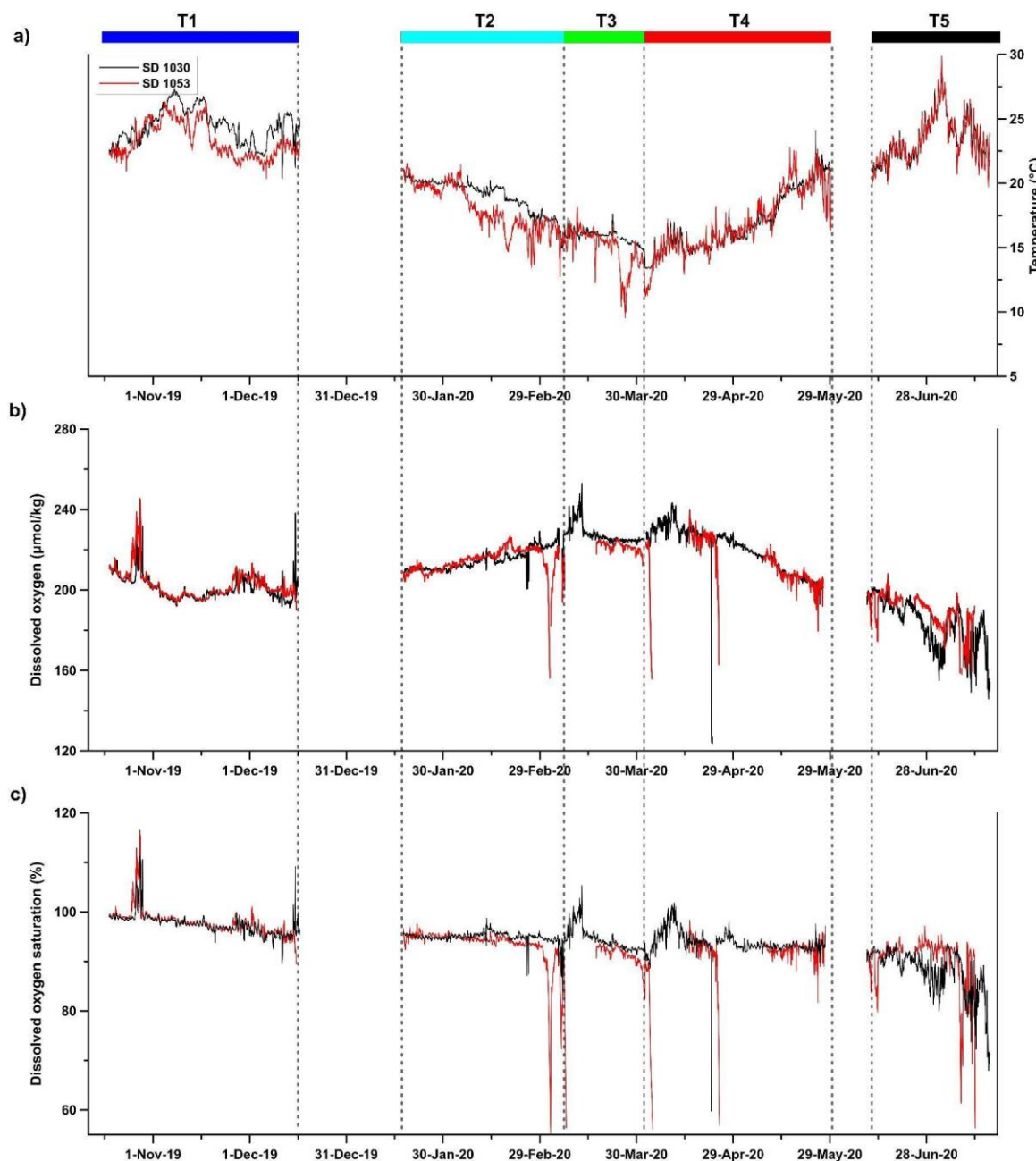
Figure 4. (a) Temperature, (b) dissolved oxygen concentration, and (c) dissolved oxygen saturation for the SD raw data (SD 1030 black line and SD 1053 red line).

Prior to applying correction all the outliers were excluded. After the first analysis we proceeded to correct the
dissolved oxygen data, using the same oxygen correction method as used in the Argo program (Bittig et al., 2018).
The principle of this method is to compare the dissolved oxygen measurements performed while the Argo oxygen
sensor is in air with the oxygen partial pressure (pO_2) in air (Johnson et al., 2015). The latter variable is easily
calculated from air temperature, air pressure, and relative humidity acquired by the SDs. Considering that the SD
oxygen sensor is installed on the hull about 0.5 m below sea surface and that the SDs sailing cause mixing of the

255 water surface while sailing, we assume that the SDs oxygen sensors were in equilibrium with the atmosphere
256 above, and furthermore, we can correct for the oxygen sensor drift using the in air calibration method (Bittig et al.,
257 2018; Johnson et al., 2015). Specifically, we computed vapour pressure (V_p, in hPa) from the empirical equation
258 reported in the operating manual of Aanderaa oxygen optode (model 4330) using the air temperature (T_{sd}) recorded
259 from SDs:

260 $$V_p = e^{(52.57-(\frac{6690.90}{T_{sd}+273.15}))-4.681*ln^{T_{sd}}+273.15} \quad (1)$$

261 and expected partial pressure (E_{PP}, in hPa) from volume fraction of oxygen (V_{fO2}=0.20946; Glueckauf, 1951),
262 atmospheric pressure (AP_{sd}), vapour pressure (V_p) and relative humidity (RH_{sd}), as follows:

263 $$E_{PP} = V_{fO2} * (AP_{sd} - (V_p * \frac{RH_{sd}}{100})) \quad (2)$$

264 The E_{PP} was then compared to the pO_2 from the SDs to compute the gain factor (G) for daily correction.

265 $$G = \frac{E_{PP}}{pO2_{sd}} \quad (3)$$

266 The corrected oxygen concentration ($O2_{csd}$) from the SDs was calculated from adjusting the oxygen data from SDs
267 ($O2_{sd}$) with the gain factor.

268 $$O2_{csd} = G * O2_{sd} \quad (4)$$

269 For each transect the mean gain was calculated and then, the gain factor was multiplied by the hourly oxygen
270 data allowing to correct the time series.
271

272 **3.3 Correction and adjustment of pCO$_2$ data**

273 **3.3.1 Fixed-sites pCO$_2$ data acquisition and qualification**

274 The pCO_2 measurements from the different fixed ocean stations were regularly compared to the pCO_2 calculated
275 from discrete water samples collected by the fixed stations and analysed for TA, pH, and DIC. During the last half
276 of the ATL2MED demonstration experiment, this routine was hampered due to COVID-19 restrictions, thus,
277 between March and July 2020, there were fewer discrete carbon samples for comparison with fixed station pCO_2.
278 Furthermore, there was minor variability in sampling frequency with regards to the fixed station pCO_2
279 measurements and in the pair of measured variables used for pCO_2 calculation (TA-pH or DIC-TA) between the
280 different fixed ocean stations (see Table S2 and S4). During the ATL2MED demonstration experiment, DIC, TA,
281 and pH were analysed according to SOP 2, 3b, and 6b, respectively (Dickson et al., 2007) with some minor local
282 variations (Table S4). Certified Reference Material (CRM) and TRIS provided by Prof. A. Dickson (Scripps,
283 USDC, USA) were used to determine the accuracy. pCO_2 was calculated using the speciation software CO2SYS
284 (Pelletier et al., 2007), with the discrete carbon pairs TA-pH or DIC-TA as input variables. In the computation, the
285 carbonate system constants from Lueker et al. (2000), the HSO_4^- constant from Dickson (1990), the total borate-
286 salinity relationship of Lee et al. (2010), and the hydrogen fluoride constant K_F from Perez and Fraga (1987) were
287 used. The uncertainties connected to this calculation ranged from 1.82% when using TA-pH as input variables to
288 2.65% when DIC-TA were the input variables (Orr et al., 2018). Based on this, no adjustments were performed
289 for the fixed station pCO_2 data when the deviation from pCO_2 calculated from discrete carbon data were less than
290 7.5 µatm and 10 µatm for the discrete carbon pairs TA-pH and DIC-TA, respectively. Uncertainty thresholds were
291 set based on measurement uncertainties at each facility and temperature and pCO_2 in the vicinity of the fixed
292 stations.
293

3.3.2 Correction of SD CO₂ data

The general accuracy of the ASVCO2 system attached to the SD 1030 was checked by PMEL prior to deployment by comparing the results with ESRL CO_2 standards traceable to WMO standards (Sutton et al., 2014). For this test, typically 6 standard gases were used. On the return of the ASVCO2 system to PMEL, it was discovered that the span gas was adjusted too low to completely flush the detector and that this had been so during the whole ATL2MED demonstration experiment. Thus, the LI-COR had to be recalibrated at the PMEL lab and this implied that the onboard gas spanning was bypassed, and new calibration coefficients were developed. Furthermore, the pre-mission test data from the PMEL lab were reprocessed using the new calibration coefficients. Based on the reported issues with the ASVCO2 instrument, the accuracy of the CO_2 measurements is estimated to be < 5 µatm. Laboratory tests of the ASVCO2 system on SD platforms highlighted an uncertainty of less than 2 µatm (Table 3 in Sutton et al., 2014).

4 Results and discussion

4.1 Salinity

Figure 5. Salinities corrected from SD 1030 (black line), and SD 1053, (red line), and *in situ* platforms (Argo floats, RV Ucadiz, gliders, and fixed stations; yellow diamonds) over the SD trajectory. The shaded grey area indicates the distance (km) between the SD trajectories. The coloured rectangles on top of the figure represent the different transects.
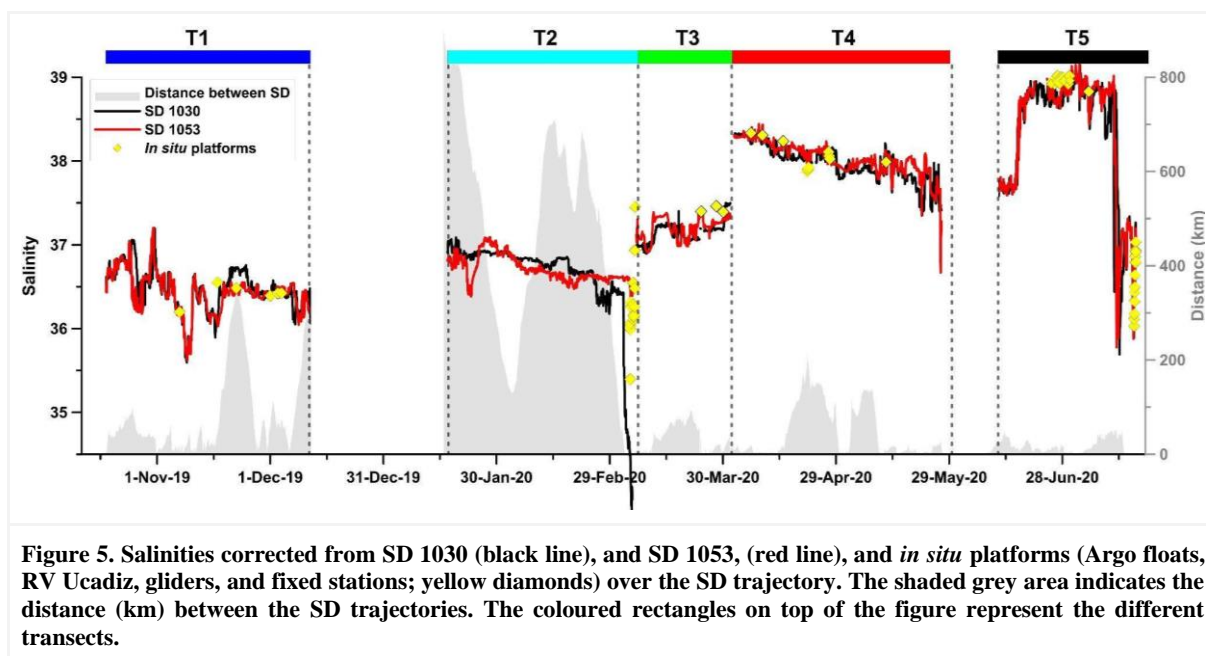
The salinity correction was based on the significant linear correlation (Fig. 3) observed across the different periods (Table 2). The periods characterised by small differences in salinity (<0.1) were not corrected. In general, the corrected salinity for both SDs showed similar values (Fig. 5), and the major differences between the two SDs were mainly due to their temporal and spatial distance. Overall, the correction was largest for SD 1053 (see RMSE values in Table 2). To validate the salinity corrected data a comparison with different observing systems was done.

For SD1030, the corrected salinity data showed a slight overestimation of salinity, while the raw salinity data showed an underestimation. The SD 1030 salinity highlights good agreement in T1 with respect to the SD 1053 (Fig. 5), the average difference was less than 0.05, the highest difference between Argo float data and corrected salinity data observed on 17 November 2019 was ~0.15. In T2, the comparison can only be made for SD 1030 with only one Argo float profile.

Between T2 and T3 a drop in salinity was observed when the SDs crossed the ETNA area, where the salinity exhibits a strong variability (Reverdin et al., 2007), triggered by freshwater flux and eddy transport (Gordon and Giulivi, 2014). This salinity drop was also observed in the climatological data (Fig. 2).

The salinity in T2 (SD 1030) only slightly differed (ΔS ~0.05) with respect to the model and values were in agreement with the observations of the Argo floats during the crossing of the Gibraltar strait. In T3 a significant

325 difference was observed between model and observation (RMSE = 0.906; Table 2), while T4 was in line with the
326 climatology as well as the fixed stations. In T5, the RMSE was 0.279 (Table 2), in the southern Adriatic, the SDs
327 spent four days sampling the area, which allowed a robust comparison between data from the E2M3A fixed ocean
328 station and the glider measurements. The comparison showed a very good agreement between the observations,
329 which had almost the same salinity. In the northern Adriatic (T5), the comparison with *in situ* data showed the
330 highest differences with respect to the other *in situ* platforms comparison. However, the comparison with the fixed
331 stations (MIRAMARE and PALOMA) showed the same temporal changes with an average difference between
332 the SDs and the MIRAMARE fixed ocean station of ~0.3.
333 Regarding SD 1053, the comparison with the different fixed ocean stations shows that the corrected salinity
334 in T2, T3, T4 and T5 are consistent with the values measured at the stations (Argo float, glider, buoy, and RV
335 Ucadiz), the differences being mainly due to the distance between the different observatories and to the natural
336 variability of the areas. Also, the corrected data fit well with climatological values and *in situ* platforms.
337 Considering that during T1 the SDs raw data showed a smaller deviation from the Argo float data, the salinity
338 correction was applied after this transect (*i.e.*, from the start of T2).

4.2 Dissolved oxygen

340 For dissolved oxygen concentration, it would have been preferable to be able to compare the SD data to discrete
341 data. However, over the period of the ATL2MED demonstration experiment, no discrete dissolved oxygen
342 measurements were available due to COVID-19 restrictions. The corrected oxygen measurements (Fig. 6a)
343 spanned from 170 µmol/kg to 270 µmol/kg highlighting the highest concentrations during spring 2020. Time series
344 of percent dissolved oxygen saturation did not show any significant trend (Fig. 6b). Oversaturation was observed
345 at the end of October 2019 (~115%) and at the beginning of March 2020 (~ 105%), while strong undersaturation
346 was observed at 1-2 of April 2020 (~95%) and 8-11 July 2020 (~92%).
347 Furthermore, we evaluated the change in dissolved oxygen measured by the two SDs in two different
348 geographical areas (the Canary Islands area and the Balearic basin), where dissolved oxygen showed
349 oversaturation (Fig. 7) and undersaturation (Fig. 8). In the first region, we made use of Chl-a data and temperature,
350 while in the second region, temperature was used to evaluate the representativeness of the correction with respect
351 to ecosystem dynamics. The optical sensors on the SDs and thus, the Chl-a measurements, were strongly affected
352 by biofouling for most of the demonstration experiment, which is why we do not use these measurements in this
353 work. However, during the 10 first days in October 2019, the Chl-a data acquired by the SDs seemed to produce
354 reasonable values in accordance with Delory et al. (2018), who found that for new sensors the increase in
355 biofouling needs weeks to become significant. We refer to these Chl-a data, collected by the SDs in the transect
356 T1, when explaining the dissolved oxygen oversaturation episode off the Canary Islands.
357 The oxygen saturation concentration can be expressed as a function of salinity and temperature, in terms of
358 solubility (Garcia and Gordon, 1992). The gas concentration in seawater depends on thermohaline characteristics
359 and biological activity. The solubility of oxygen decreases with increasing temperature and salinity, showing a
360 strong correlation. In the ocean, dissolved oxygen saturation lower than 100% can be observed during the cold
361 seasons while in the warm season oxygen saturation is higher than 100%, inversely to the dissolved oxygen
362 concentrations (i.e., high concentrations during cold season and low in the warm season). This is because heating
363 and cooling are generally faster than outgassing, except for episodes of high wind speeds which intensifies the air-
364 sea gas exchange (Ulses et al., 2021). Furthermore, dissolved oxygen concentration is affected by primary
365 production and respiration.

366
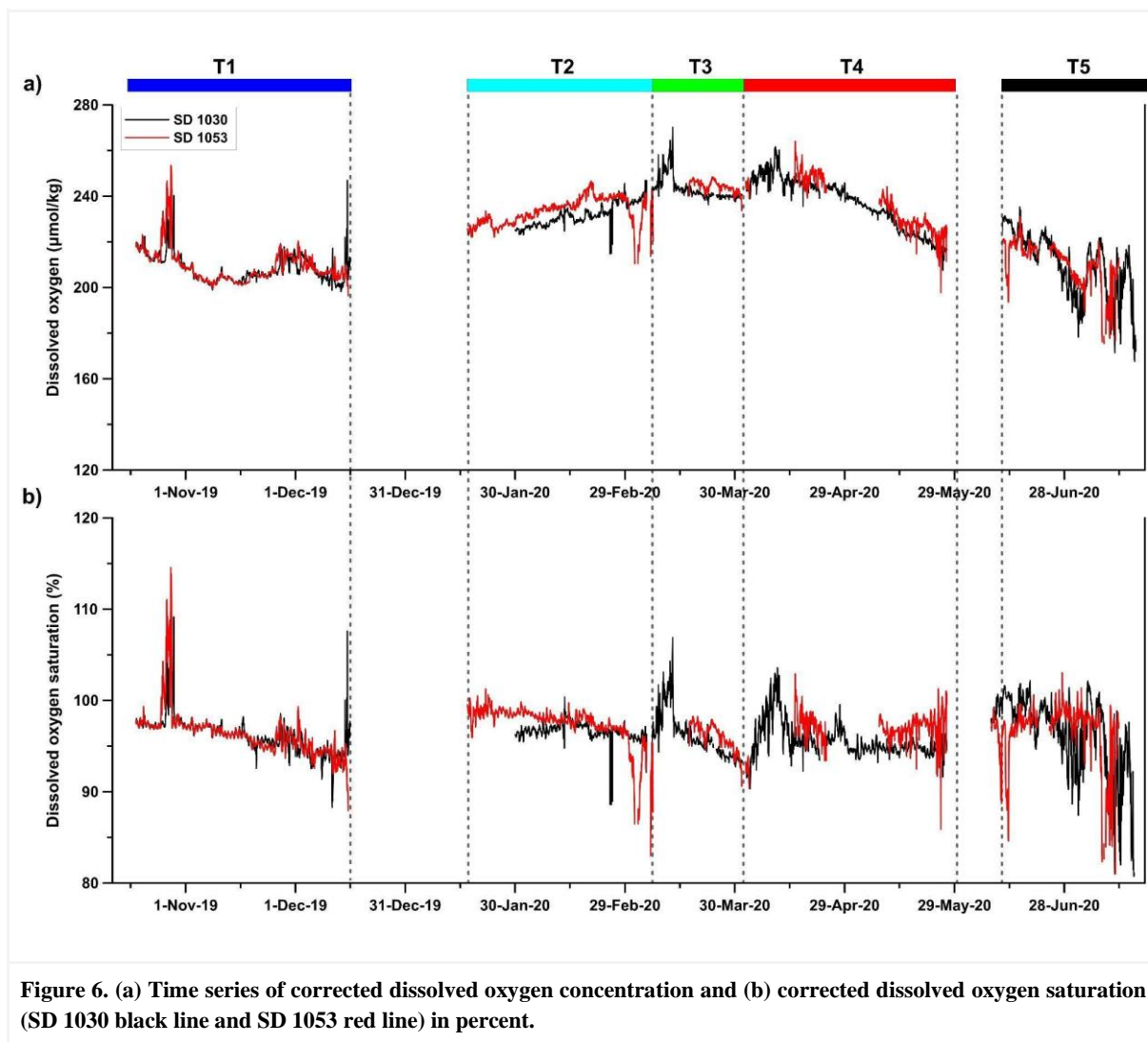
Figure 6. (a) Time series of corrected dissolved oxygen concentration and (b) corrected dissolved oxygen saturation (SD 1030 black line and SD 1053 red line) in percent.

367

368   Between 25 and 29 October, the dissolved oxygen concentration and saturation were high around the Canary
369   Islands (>240 µmol/kg and >110%; Fig. 7a and b). During the same period high concentrations of Chl-a were
370   measured by SDs (~ 2 µg/l, Fig. 7b, blue and orange line). The area with high Chl-a concentrations off the Canary
371   Islands was visible on the satellite images of sea surface Chl-a concentration (Fig. 7c) and at the same time low
372   sea surface temperature was observed (Fig. 7d). High Chl-a concentrations and low temperatures identify a
373   mesoscale structure that has moved away from the African shelf. Considering that the latter is a very productive
374   area due to the permanent upwelling off NW Africa coast (Cropper et al., 2014; Fischer et al., 2016), this justifies
375   the high Chl-a concentration observed by the SDs at that time.
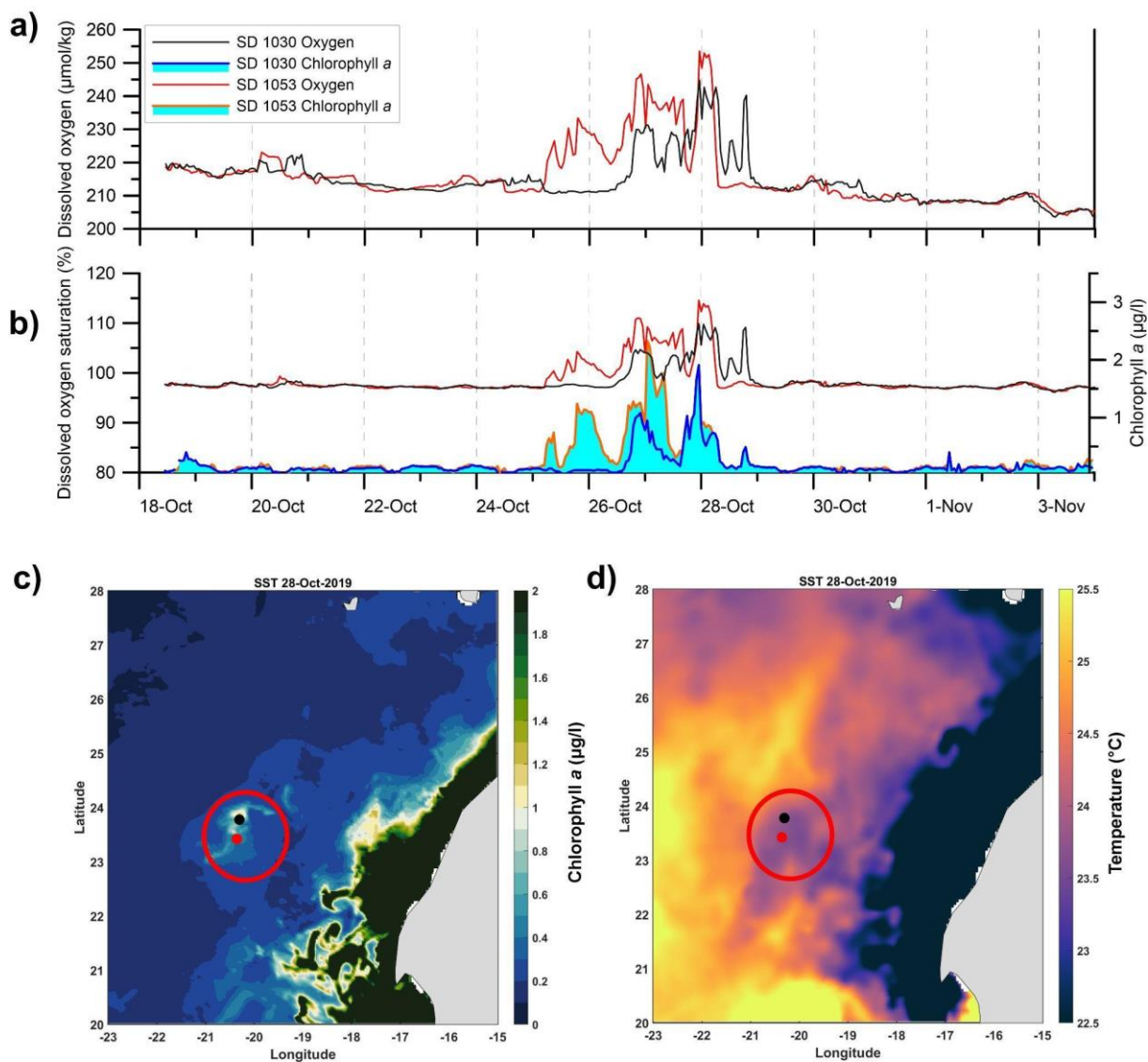
Figure 7. Time series of (a) dissolved oxygen concentration and (b) dissolved oxygen saturation in the Canary Islands area. Sea surface Chl-a concentration (c), and (d) sea surface temperature on 28 October 2019. The red circle highlights the position of SDs (black dot = SD1030 and red dot=SD1053).

383
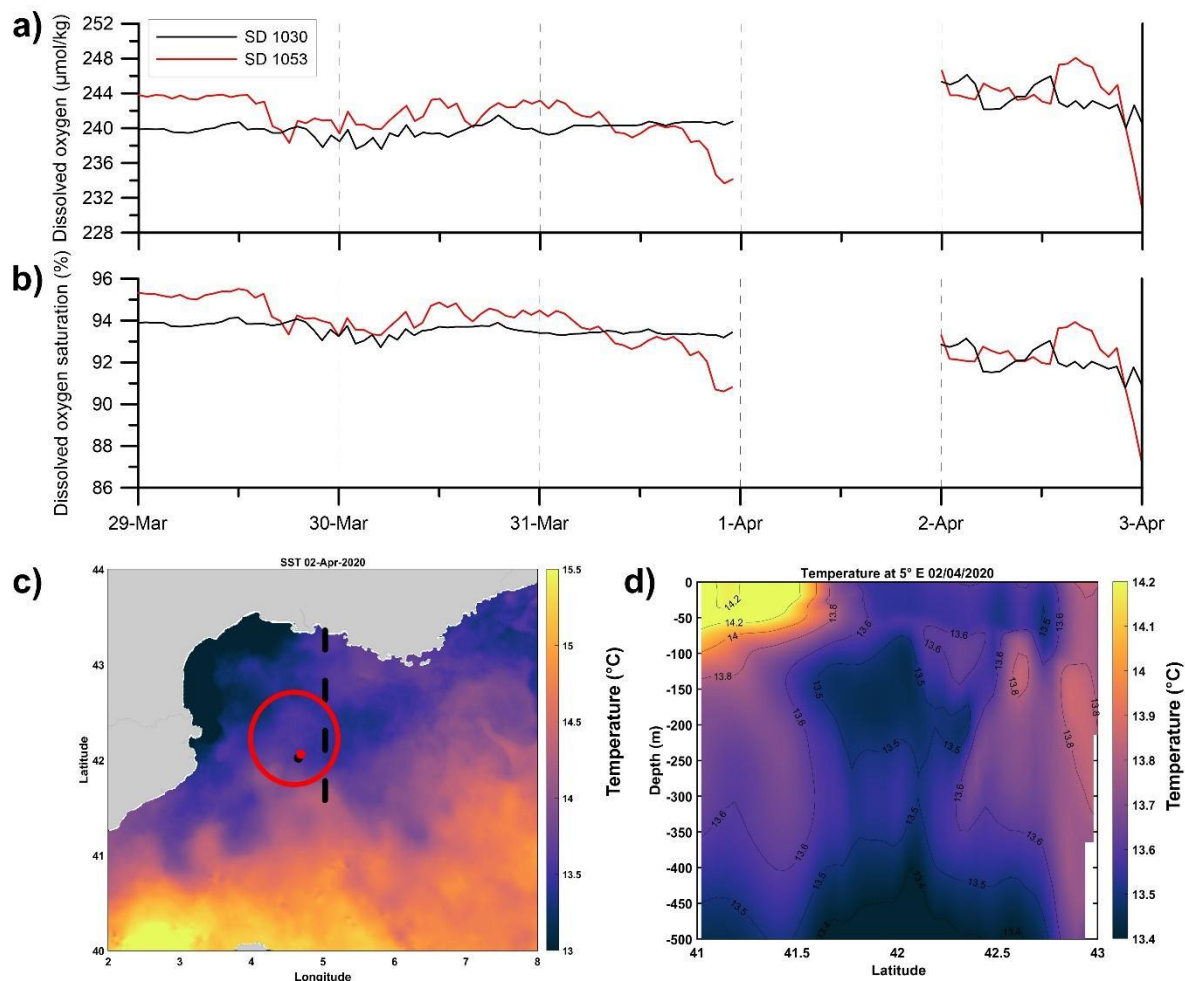
384
385 **Figure 8. Time series of (a) dissolved oxygen concentration and (b) percent dissolved oxygen saturation in the Balearic**
386 **basin. (c) Sea surface temperature evolution between 31 March and 2 April 2020. The black dotted line highlights the**
387 **vertical section in (d). The red circle highlights the position of SDs (black dot = SD1030 and red dot=SD1053).**
388

389 Between 29 March and 3 April 2020, the SDs crossed the Balearic basin reaching the Gulf of Lion on 1 April
390 2020, the SD 1053 measured a decrease in dissolved oxygen concentrations of about 10 µmol/kg (Fig. 8a). This
391 behaviour was also observed in the dissolved oxygen saturation (Fig. 8b) which reached values lower than 95%.
392 The northern part of the basin was characterised by lower surface temperatures (Fig. 8c) than the southern part.
393 The vertical temperature section (Fig. 8d) highlighted the presence of upwelling of cold water to the surface
394 justifying the lower surface temperature observed in Fig. 8c. The presence of this upwelled water caused the
395 decrease in dissolved oxygen saturation (Fig. 8b) observed by the SDs, as the upwelled water is commonly
396 characterised by low dissolved oxygen concentrations due to biological respiration (Chan et al., 2019).
397

398 **4.3 pCO$_2$**

399 pCO$_2$ (in µatm) from the ASVCO2 instrument attached to the SD 1030 were calculated according to Sutton et al.
400 (2014) using T and S from the SBE37-SMP-ODO at the SD. Fig. 9a shows the uncorrected and corrected pCO$_2$
401 acquired from the SD 1030. In Fig. 9b, the difference between corrected and uncorrected pCO$_2$ is shown and the
402 offset increases from approximately 1 µatm at the start of the experiment to approximately 12 µatm at the end.
403
404
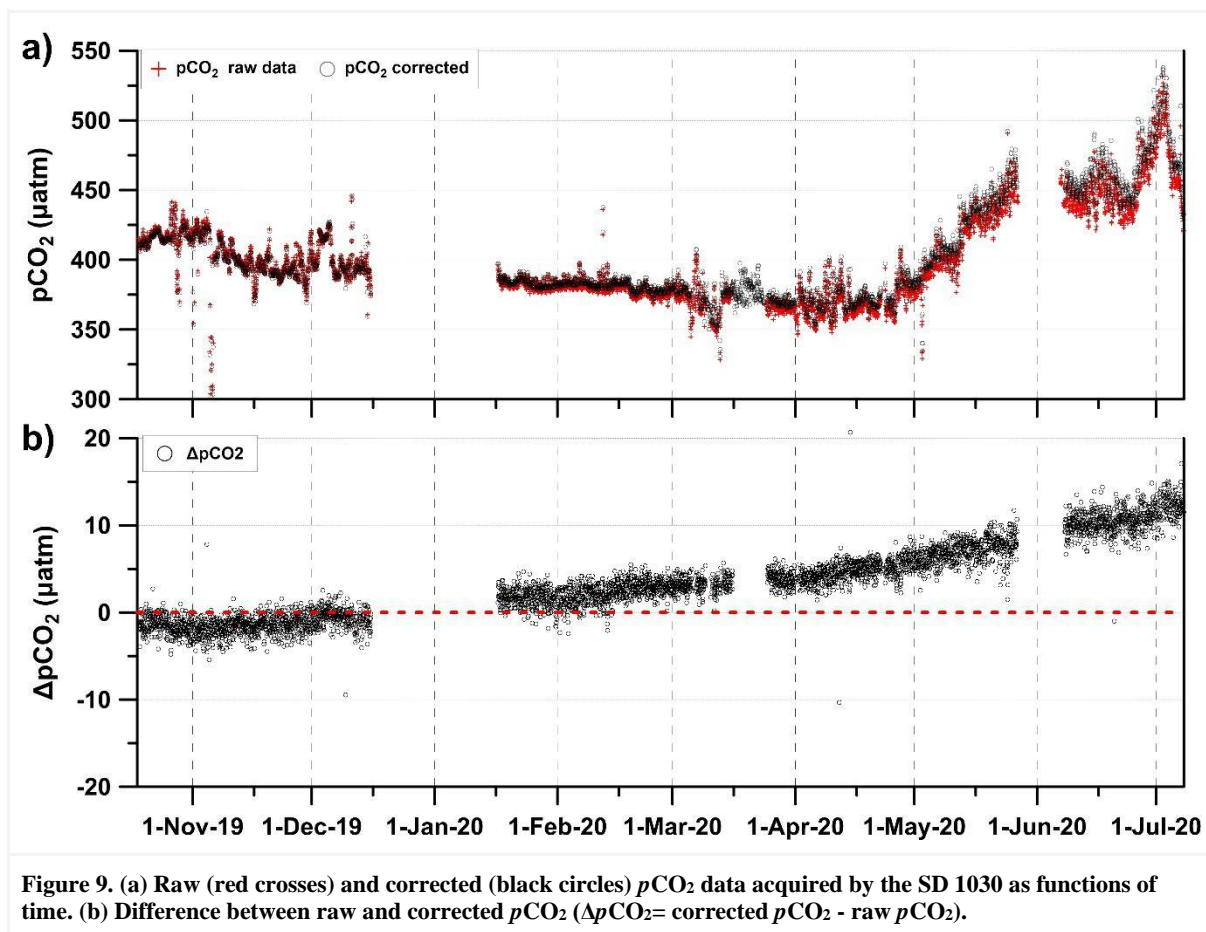
Figure 9. (a) Raw (red crosses) and corrected (black circles) pCO$_2$ data acquired by the SD 1030 as functions of time. (b) Difference between raw and corrected pCO$_2$ (ΔpCO$_2$= corrected pCO$_2$ - raw pCO$_2$).

405

406   The pCO$_2$ sensors at the different fixed stations were deployed at depths between 2 to 10 m while the SD measured
407   at 0.5 m depth. To be able to compare pCO$_2$ measurements from the different depths, the station pCO$_2$ data were
408   normalised to surface temperature by using the relationship of Takahashi et al. (1993): $pCO_2(1) =$
409    $pCO_2(2) \, exp^{0.0423(T_1-T_2)}$ (5)
410   where T is temperature and 1 and 2 refer to the measurements at 0.5 m depth of the SD and at the measurement
411   depth of each local station, respectively. Furthermore, the pCO$_2$ measurements acquired by the SD 1030 were
412   compared to the corrected pCO$_2$, surface temperature normalised, from the fixed ocean stations (Fig. 10 and Table
413   3). The difference varied between -0.5 and -16.9 µatm. The largest difference occurred in the eastern Atlantic,
414   where calculated pCO$_2$ from discrete DIC and TA were compared to the SD 1030 pCO$_2$ data. Part of this deviation
415   is likely attributed to calculation errors which is estimated to about 10 µatm when errors in both DIC, TA, and the
416   carbon constants are included (Orr et al., 2018). The smallest difference between the SD 1030 pCO$_2$ and the pCO$_2$
417   acquired from the fixed stations and normalised to surface temperature are seen at DYFAMED toward the end of
418   April 2020 (-2.9 µatm) and at MIRAMARE in mid July 2020 (-0.5 µatm). The larger discrepancy at W1M3A and
419   PALOMA might be attributed to processes which are not taken into account by temperature normalising, *e.g.*,
420   spatial gradients due to primary production/remineralisation, which would decrease/increase the pCO$_2$. However,
421   it is difficult to estimate the impact of these processes.

422

Figure 10. Comparison between pCO$_2$ measured by the SD 1030 (blue) and at the fixed ocean stations (black and green): the fixed ocean station pCO$_2$ measured at *in situ* depth and temperature (black) and the fixed ocean station pCO$_2$ normalised to surface temperature (green). (a) DYFAMED fixed station, (b) W1M3A fixed station, (c) PALOMA fixed station, and (d) MIRAMARE fixed station.
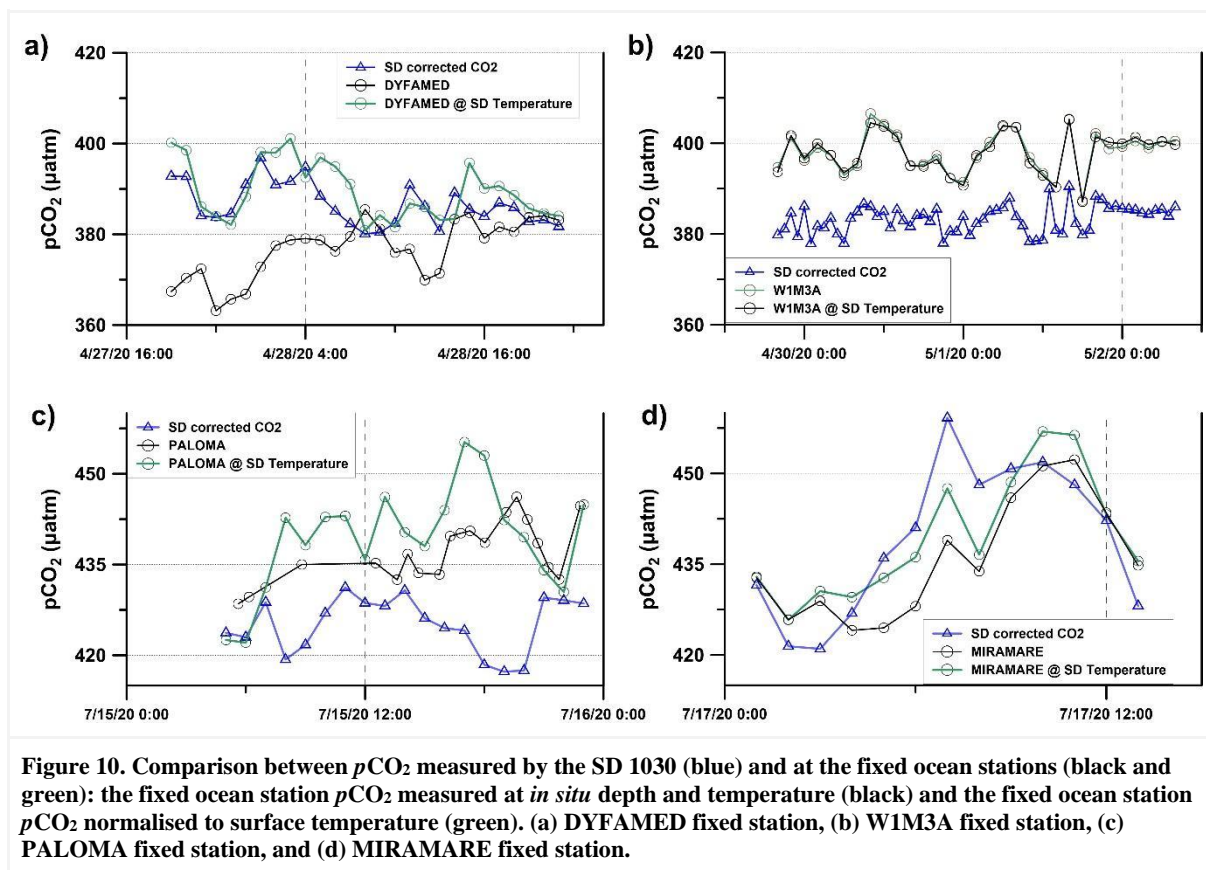
423
424

425   To assess the representativeness of the pCO$_2$ correction in terms of ecosystem dynamics, a comparison was made
426   between the corrected pCO$_2$, temperature, and Chl-a concentrations from satellites. The pCO$_2$ in seawater is
427   influenced by primary production, respiration, air-sea gas exchange, formation and dissolution of calcium
428   carbonates, water mixing, riverine discharges and advection (Zeebe and Wolf- Gladrow, 2007; Bauer et al., 2013;
429   Millero 2007), which leads to significant variations in different regions. The temperature affects the pCO$_2$ through
430   the thermodynamic dissociation constants of the carbonic acids, which directly affects the CO$_2$ equilibria (eg.
431   Millero, 2007) and to a lesser extent also the gas solubility.
432   Throughout the ATL2MED demonstration experiment, the pCO$_2$ value (Fig. 11a) showed almost the same
433   pattern as the surface temperature (Fig. 11b), and furthermore, the pCO$_2$ values in the ETNA were lower than those
434   of the Mediterranean at the same sea surface temperature. The main reason for this difference is attributed to the
435   lower DIC in the Atlantic waters with respect to the Mediterranean (Alvarez et al., 2014).
436   We observed the highest pCO$_2$ variability in the Mediterranean Sea , as the temperature increased by more
437   than 15°C from winter to summer leading to an increase in pCO2 . A reduction in pCO$_2$ due to phytoplankton
438   photosynthesis is present at the end of the mission in the northern Adriatic where the fertilisation by nutrients
439   carried by the Po river induced an increase in Chl-a concentrations (green line in Fig. 11b).

440
441
442
443
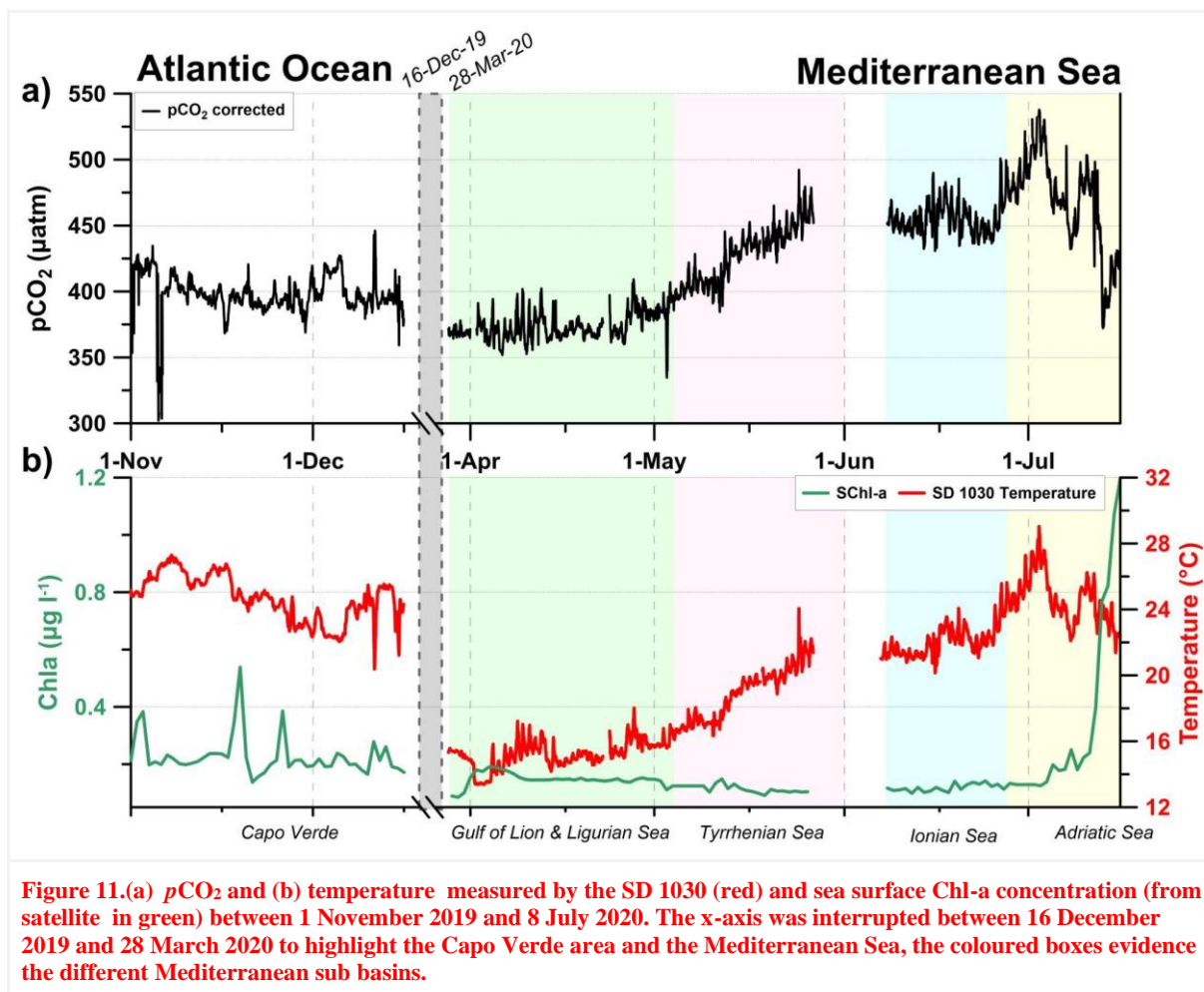
Figure 11.(a) pCO$_2$ and (b) temperature measured by the SD 1030 (red) and sea surface Chl-a concentration (from satellite in green) between 1 November 2019 and 8 July 2020. The x-axis was interrupted between 16 December 2019 and 28 March 2020 to highlight the Capo Verde area and the Mediterranean Sea, the coloured boxes evidence the different Mediterranean sub basins.

444

445

446   **Table 3. Comparison between pCO$_2$ measurements at SD 1030 and the fixed ocean stations.**

Station/ platform	Measurements	Date	Deviation between pCO$_2$ at SD 1030 and pCO$_2$ at fixed station normalised to SST (µatm)
RV Meteor	Discrete DIC and TA samples @ 5 m	30 Nov 2019	-16.9 µatm
DYFAMED	pCO$_2$ sensor @ 10 m	27-28 Apr 2020	-2.9 µatm
W1M3A	pCO$_2$ sensor @ 6 m	28 Apr - 2 May 2020	-14.2 µatm
PALOMA	pCO$_2$ sensor @ 3 m	15 July 2020	-14.7 µatm
MIRAMARE	pCO$_2$ sensor @ 2 m	17 July 2020	-0.5 µatm

447   SST= sea surface temperature

448

5 Summary

450   The ATL2MED demonstration experiment, which lasted for 273 days, represented the first monitoring

451   experiments of SDs covering both the ETNA region and the Mediterranean Sea, evaluating dynamics between

452   fixed ocean stations within the same basin as well as comparing characteristics between basins. The experiment

453   covered all seasons with varying meteorological and oceanographic conditions, primary productivity, and maritime

454 traffic. The ATL2MED lasted longer than planned primarily due to challenges with heavy biofouling of the two
455 SDs, COVID-19 pandemic restrictions, low winds, and strong contrary winds.

456   A huge amount of data has been produced during the ATL2MED demonstration experiment, and the data
457 required quality control and assurance to a varying degree, primarily depending on how sensitive the sensors were
458 to biofouling. Due to the COVID-19 pandemic restrictions, there was a lack of validation samples collected from
459 cruise transects, Argo floats, and fixed stations, and this has enforced a new way of thinking regarding drift
460 correction. The SBE salinity data acquired by the SDs have been corrected, when necessary, using model products
461 and the method was validated by comparing the data corrected with available *in situ* measurements. This resulted
462 in remarkable consistency in the corrected salinity values between both SDs. Data from the Aanderaa dissolved
463 oxygen sensors mounted on the SDs were corrected making use of in air oxygen measurements to correct for the
464 erroneous trend in O_2 saturation (%). The pCO$_2$ data from SD 1030 were corrected at PMEL and compared with
465 pCO$_2$ data acquired from fixed ocean stations. The corrected SD datasets fit well with the data from fixed stations
466 and gliders, which means that the correction methods used are valid. The output is datasets that are available for
467 process interpretations in future research.

468   Other SD sensors were affected by biofouling to such a degree that the datasets were unable to be corrected
469 given the limited samples available for validation, like *e.g.* the optical sensors for fluorescence measurements.
470 Some recommendations related to this issue are presented in the next section.

471   The ATL2MED demonstration experiment is an example of how ASV can be used to perform multi-variable
472 and high-resolution sampling from areas which are not easily accessible, *e.g.* due to remote location, limited
473 shiptime availability, or COVID-19 restrictions. The SDs are environmentally friendly platforms, and they,
474 together with other ASV, are useful as a complement in the validation of fixed ocean stations. However, the
475 experiment clearly shows some of the challenges faced when this type of surface vehicle is part of long-term
476 missions.

477

6 Experiences and recommendations

479 Our experiences and recommendations from the ATL2MED demonstration experiment can be summarised in the
480 following bullet points, which are explained in more detail at the end of this paragraph:

481 We experienced that

482   -   the SD sensors were exposed to severe biofouling
483   -   a substantial amount of effort was required to correct the SD datasets
484   -   some of the SD sensors were mounted in an unfavourable way
485   -   the COVID-19 pandemic limited the access to ship time and thus impacts on the collection of discrete
486   validation samples

487 We recommend to

488   -   ensure a maintenance and cleaning frequency of the SD sensors and the hull that is adapted to the local
489   environment
490   -   use of biolimiting equipment at the SDs
491   -   implement an automatic in air calibration procedure for SD oxygen measurements
492   -   ensure that the SD sensors are mounted in such a way that they are exposed to open water
493   -   ensure that a sufficient amount of independent measurements (*e.g.*, salinity, dissolved oxygen, carbonate
494   system, Chl-a) are collected in the vicinity of the SD trajectories in order to validate the SD sensors

495 In general, the use of SDs requires considerable effort to ensure that the data are of scientifically usable quality, as
496 these vehicles operate on the surface and are more exposed to biofouling. For future trials, a frequency of sensor
497 cleaning and hull maintenance cleaning should be introduced depending on the monitoring area. In situations
498 where this is not possible, bio-limiting devices should be used, such as UV systems and wipers powered by the
499 solar panels that regularly clean the optical sensors. Experience from the ATL2MED demonstration experiment
500 has shown that the SBE37 sensors appear to be reliable and robust with respect to biofouling. Regarding the
501 dissolved oxygen correction, it is recommended to perform an in-air calibration as used for Argo floats to be able
502 to correct the drift of the oxygen sensor more easily.

The ATL2MED demonstration experiment suffered from a lack of discrete samples for validation. Therefore, future experiments should be organised to collect discrete samples for acquired parameters at appropriate frequencies, which will greatly facilitate validation of the quality of the SD dataset. Finally, the suitability of SDs as a tool to validate other types of measuring platforms (e.g. fixed ocean stations, mobile devices or ships) strongly depends on various conditions, such as the distance to the platforms, the depth of measurements at fixed stations and the environmental conditions. All these factors need to be carefully considered to ensure the best possible data set for such a validation.

Data availability. Data described in this work is available from different sources, see Table S6 in the Supplementary Material.

Supplement. The supplementary material is available at the end of this manuscript.

Author contribution. R. M: Data curation, Investigation, Validation, Visualization, Writing – original draft, Writing – review & editing, Conceptualization, Formal analysis, Methodology, Software. M. G.: Investigation, Validation, Methodology, Writing – original draft, Writing – review & editing, Conceptualization, Formal analysis. E. M.: Writing – original draft, Writing – review & editing, Funding acquisition, Resources. L. C. : Methodology, Writing – review & editing, Funding acquisition, Investigation. M. P.: Writing – review & editing, Investigation, Data curation. M. F.: Writing – review & editing, Investigation, Data curation. S. P.: Writing – review & editing, Investigation, Data curation. V. C.: Writing – review & editing, Conceptualization , Funding acquisition, Resources. C. D.: Writing – review & editing, Investigation, Data curation. R. B.: Writing – review & editing, Data curation. C. C.: Writing – review & editing, Data curation. A. L.: Writing – review & editing, Data curation. A. I.: Writing – review & editing, Data curation. M. B.: Writing – review & editing, Data curation. I. S.: Data curation, Investigation, Validation, Visualization, Writing – original draft, Writing – review & editing, Conceptualization , Methodology, Funding acquisition, Project administration, Resources.

Competing interests. The contact author declares that none of the authors has any competing interests.

Acknowledgement

The ATL2MED experiment has received generous funding from the US company PEAK 6 Invest and invaluable support regarding coordination, operation, and data deliverance from Saildrone Inc.. Furthermore, funding has been provided by GEOMAR Helmholtz Centre for Ocean Research (GEOMAR), Integrated Carbon Observation System - Ocean Thematic Centre (ICOS-OTC), the French National Centre for Scientific Research (CNRS), Oceanography Laboratory of Villefranche (LOV), the Oceanic Platform of the Canary Islands (PLOCAN), Ocean Science Centre Mindelo (OSCM), the Hydrographic Institute of Portugal (IH), Balearic Islands Coastal Observing and Forecasting System (SOCIB), Italian National Institute of Oceanography and Applied Geophysics (OGS), Helmholtz Zentrum Geesthacht (HZG), Centre Scientifique de Monaco (CSM), National Research Council-Institute of Marine Sciences (CNR-ISMAR), and National Research Council - Institute for the study of Anthropic Impact and Sustainability in the Marine Environment (CNR-IAS). We thank OGS engineers Paolo Mansutti and Giuseppe Siena for the assistance during the final recovery of the SDs, and Piero Zuppelli, Riccardo Gerin, Antonio Bussani and Massimo Pacciaroni for piloting the OGS glider. Furthermore, we thank Björn Fiedeler and Benjamin Pfeil for initialising the demonstration experiment and for executing the first phase of the experiment. Finally, we thank Adrienne Sutton and Stacy Manner (PMEL) for invaluable help with correcting the ASVCO2 pCO$_2$ data.

545

References

Álvarez, M., Sanleón-Bartolomé, H., Tanhua, T., Mintrop, L., Luchetta, A., Cantoni, C.,Schroeder, K., Civitarese, G., 2014. The CO_2 system in the Mediterranean Sea: A basin wide perspective. Ocean Sci. 10, 69–92.

Bauer J. E., Cai W.-J., Raymond P. A., Bianchi T. S., Hopkinson C. S. & Regnier P. A. G.. 2013. The changing carbon cycle of the coastal ocean. Nature 504, 61-70.

Bittig, H. C., Körtzinger, A., Neill, C., van Ooijen, E., Plant, J. N., Hahn, J., Johnson, K. S., Jang, B., and Emerson, S. R.: Oxygen optode sensors: principle, characterization, calibration, and application in the ocean, Front. Mar. Sci., 4, 429, https://doi.org/10.3389/fmars.2017.00429, 2018.

Bosse, A., Testor, P., Mortier, L., Prieur, L., Taillandier, V., D'Ortenzio, F., and Coppola, L.: Spreading of Levantine Intermediate Waters by submesoscale coherent vortices in the northwestern Mediterranean Sea as observed with gliders, J. Geophys. Res-Oceans, 120(3), 1599-1622, https://doi.org/10.1002/2014JC010263, 2015.

Bozzano, R., Pensieri, S., Pensieri, L., Cardin, V., Brunetti, F., Bensi, M., Petihakis, G., Tsagaraki, T. M., Ntoumas, M., Podaras, D., and Perivoliotis, L.: The M3A network of open ocean observatories in the Mediterranean Sea, in: 2013 MTS/IEEE OCEANS-Bergen, IEEE, Bergen, Norway, 10-14 June 2013, 1-10, 2013.

Bozzano, R. and Pensieri, S.: W1M3A fixed station data collected as part of the ATL2MED demonstration experiment 2019-2020 [Data set], https://hdl.handle.net/11676/Z9bGSnVObyglR0o8zcvmIXBz, 2024.

Buongiorno Nardelli, B., Tronconi, C., Pisano, A., and Santoleri, R.: High and Ultra-High resolution processing of satellite Sea Surface Temperature data over Southern European Seas in the framework of MyOcean project, Copernicus Monitoring Environment Marine Service (CMEMS) [Data set], https://doi.org/10.48670/moi-00172, 2022.

Canepa, E., Pensieri, S., Bozzano, R., Faimali, M., Traverso, P., and Cavaleri, L.: The ODAS Italia 1 buoy: More than forty years of activity in the Ligurian Sea, Progr. Oceanogr., 135, 48-63, https://doi.org/10.1016/j.pocean.2015.04.005, 2015.

Cantoni, C., Luchetta, A., Celio, M., Cozzi, S., Raicich, F., and Catalano, G.: Carbonate system variability in the gulf of Trieste (north Adriatic Sea), Estuar. Coast. Shelf. S., 115, 51–62, https://doi.org/10.1016/j.ecss.2012.07.006, 2012.

Cantoni, C. and Luchetta, A.: PALOMA fixed station data collected as part of the ATL2MED demonstration experiment 2019-2020 [Data set], https://hdl.handle.net/11676/an-PJSKTiEVHj3H0gA8ak3lG, 2024.

Capó, E., McWilliams, J. C., Mason, E., and Orfila, A.: Intermittent frontogenesis in the Alboran Sea. *Journal of Physical Oceanography*, *51*(5), 1417-1439, 2021.

Cardin, V., Ursella, L., Siena, G., Brunetti, F., Kuchler, S., and Partescano, P.: E2M3A-2017-2019-CTD-time-series-South Adriatic [Data set], https://nodc.ogs.it/catalogs/doidetails;jsessionid=9D31FDE64403D9BF54F05A1F03D45FB1?0&doi=10.6092/d0d50095-bd30-4ff7-8d0a-a12121e72f78, 2020.

Chan, F., Barth, J. A., Kroeker, K. J., Lubchenco, J., and Menge, B. A.: The dynamics and impact of ocean acidification and hypoxia. Oceanography, 3*2*(3), 62-71, 2019.

Civitarese G., Gačić M., Batistić M., Bensi M., Cardin V., Dulčić J., Garić R., Menna M.. The BiOS mechanism: history, theory, implications. Progress in Oceanography, 103056. 2023.

Clayton, T. D. and Byrne, R. H.: Spectrophotometric seawater pH measurements: total hydrogen ion concentration scale calibration of *m*-creosol purple and at-sea results. Deep-Sea Res., 40, 2115-2129, 1993.

Clementi, E., Aydogdu, A., Goglio, A. C., Pistoia, J., Escudier, R., Drudi, M., Grandi, A., Mariani, A., Lyubartsev, V., Lecci, R., Cretí, S., Coppini, G., Masina, S., and Pinardi, N.: Mediterranean Sea Physical Analysis and Forecast (CMEMS MED-Currents, EAS6 system) (Version 1), Copernicus Monitoring Environment Marine Service (CMEMS) [Data set], https://doi.org/10.25423/CMCC/MEDSEA_ANALYSISFORECAST_PHY_006_013_EAS7, 2021.

Coppola, L., Raimbault, P., Mortier, L., and Testor, P.: Monitoring the environment in the northwestern Mediterranean Sea, Eos, 100, https://doi.org/10.1029/2019EO125951, 2019.

Coppola, L., Diamond, R. E., Carval, T., Irisson J. O., and Desnos, C.: Dyfamed observatory data, SEANOE [Data set], https://doi.org/10.17882/43749, 2023.

Cropper, T. E., Hanna, E., and Bigg, G. R.: Spatial and temporal seasonal trends in coastal upwelling off Northwest Africa, 1981–2012, Deep-Sea Res. Pt. I, 86, 94-111, https://doi.org/10.1016/j.dsr.2014.01.007, 2014.

Delauney, L., Compère, C., and Lehaitre, M.: Biofouling protection for marine environmental sensors, Ocean Sci., 6, 503–511, https://doi.org/10.5194/os-6-503-2010, 2010.

Delory, E., and Jay P., (Eds.): Challenges and Innovations in Ocean *In Situ* Sensors: Measuring Inner Ocean Processes and Health in the Digital Age. Elsevier, 408 pp, ISBN: 9780128098868, 2018.

Dickson, A. G.: Standard potential of the reaction: AgCl(s) + ½H2(g) = Ag(s) + HCl(aq), and the standard acidity constant of the ion HSO4 – in synthetic sea water from 273.15 to 318.15 K, J. Chem. Thermodyn., 22, 113–127, https://doi.org/10.1016/0198-0149(90)90004-F, 1990.

Dickson, A. G. and Goyet, C.: Handbook of methods for the analysis of the various parameters of the carbon dioxide system in sea water. Version 2, Oak Ridge National Lab. (ORNL), https://doi.org/10.2172/10107773, 1994.

Dickson, A. G., Sabine, C. L., and Christian, J. R. (Eds): Guide to best practices for ocean CO2 measurements, PICES Special Publication 3, North Pacific Marine Science Organization Sidney, British Columbia, 191, https://doi.org/10.25607/OBP-1342, 2007.

Edmond, J. M. . High precision determination of titration alkalinity and total carbon dioxide content of sea water by potentiometric titration. In *Deep Sea Research and Oceanographic Abstracts* (Vol. 17, No. 4, pp. 737-750). Elsevier. 1970.

Escudier, R., Clementi, E., Cipollone, A., Pistoia, J., Drudi, M., Grandi, A., Lyubartsev, V., Lecci, R., Aydogdu, A., Delrosso, D., Omar, M., Masina, S., Coppini, G., and Pinardi, N.: A High Resolution Reanalysis for the Mediterranean Sea, Front. Earth Sci., 9, https://doi.org/10.3389/feart.2021.702285, 2021.

Escudier, R., Clementi, E., Omar, M., Cipollone, A., Pistoia, J., Aydogdu, A., Drudi, M., Grandi, A., Lyubartsev, V., Lecci, R., Cretí, S., Masina, S., Coppini, G., and Pinardi, N.: Mediterranean Sea Physical Reanalysis (CMEMS MED-Currents) (Version 1) [Data set], Copernicus Monitoring Environment Marine Service (CMEMS), https://doi.org/10.25423/CMCC/MEDSEA_MULTIYEAR_PHY_006_004_E3R1I, 2020.

Fischer, G., Romero, O., Merkel, U., Donner, B., Iversen, M., Nowald, N., Ratmeyer, V., Ruhland, G., Klann, M., and Wefer, G.: Deep ocean mass fluxes in the coastal upwelling off Mauritania from 1988 to 2012: variability on seasonal to decadal timescales, Biogeosciences, 13, 3071–3090, https://doi.org/10.5194/bg-13-3071-2016, 2016.

Friederich, G. E., Brewer, P. G., Herlien, R., and Chavez, F. P.: Measurement of sea surface partial pressure of CO_2 from a moored buoy, Deep-Sea Res. Pt. I, 42, 1175–1186, https://doi.org/10.1016/0967-0637(95)00044-7, 1995.

Gačić, M., Ursella, L., Kovačević, V., Menna, M., Malačič, V., Bensi, M., Negretti, M.-E., Cardin, V., Mirko Orlić, M., Sommeria, J., Barreto, R. V., Viboud, S., Valran, T., Petelin, B., Siena, G., and Rubino, A.: Impact of dense-water flow over a sloping bottom on open-sea circulation: laboratory experiments and an Ionian Sea (Mediterranean) example. Ocean Sci., 17, 975–996, https://doi.org/10.5194/os-17-975-2021, 2021.

Garcia, H. E. and Gordon, L. I.: Oxygen solubility in seawater: Better fitting equations, Limnol. Oceanogr., 37 (6), 1307-1312, 1992.

GDAC: ftp://ftp.ifremer.fr/argo, last access 17-10-2023.

Gentemann, C. L., Scott, J. P., Mazzini, P. L. F., Pianca, C., Akella, S., Minnett, P. J., Cornillon, P., Fox-Kemper, B., Cetinić, I., Chin, T. M., Gomez-Valdes, J., Vazquez-Cuervo, J., Tsontos, V., Yu, L., Jenkins, R., De Halleux, S., Peacock, D., and Cohen, N.: Salidrone - Adaptively sampling the marine environment, BAMS, https://doi.org/10.1175/BAMS-D-19-0015.1, 2020.

Gerin, R., Bussani, A., Kuchler, S., Martellucci, R., Pacciaroni, M., Pirro, A., Zuppelli, P., and Mauri, E: OGS GLIDER MISSION Convex20 Dataset [Data set], 2021.

Giani, M.: MIRAMARE fixed station data collected as part of the ATL2MED demonstration experiment 2019-2020 [Data set], https://hdl.handle.net/11676/ngPlu-Q0dtDcDx2wMFTNOtnZ, 2024.

Glueckauf, E.: The Composition of Atmospheric Air, In: Compendium of Meteorology, edited by: Malone, T.F., American Meteorological Society, Boston, MA., 3-10, https://doi.org/10.1007/978-1-940033-70-9_1, 1951.

Gonzalez, A. I. and Bruno, M.: Data from RV Ucadiz, 5-6 March 2020 [Dataset], https://fileshare.icos-cp.eu/s/eyLp9m685QA8ME7, 2024.

648 Gordon, A. L. and Giulivi, C. F.: Ocean eddy freshwater flux convergence into the North Atlantic subtropics.
649   Journal of Geophysical Research: Oceans, *119*(6), 3327-3335, 2014.

650 Hernandez-Ayon, J. M., Belli, S. L., Zirino, A.: pH, alkalinity and total CO2 in coastal seawater by potentiometric
651   titration with a difference derivative readout, Anal. Chim. Acta 394, 101–108, 1999.

652 Johnson, K. M., Wills, K. D., Butler, D. B., Johnson, W. K. and Wong, C. S.: Coulometric total carbon dioxide
653   analysis for marine studies, Mar. Chem., 44, 167-187, 1993.

654 Johnson, K. S., Plant, J. N., Riser, S. C., and Gilbert, D.: Air oxygen calibration of oxygen optodes on a profiling
655   float array, J. Atmos. Ocean. Tech., 32, 2160-2172, https://doi.org/10.1175/JTECH-D-15-0101.1, 2015.

656 Kokkini, Z., Mauri, E., Gerin, R., Poulain, P.-M., Simoncelli, S., and Notarstefano, G.: On the salinity structure in
657   the South Adriatic as derived from float and glider observations in 2013–2016, Deep-Sea Res. Pt. II, 171,
658   104625, https://doi.org/10.1016/j.dsr2.2019.07.013, 2019.

659 Lee, K., Kim, T.-W., Byrne, R. H., Millero, F J., Feely, R. A., and Liu, Y.-M.: The universal ratio of boron to
660   chlorinity for the North Pacific and North Atlantic oceans, Geochim. Cosmochim. Acta, 74, 1801–1811,
661   https://doi.org/10.1016/j.gca.2009.12.027, 2010.

662 Lueker, T. J., Dickson, A. G., and Keeling, C. D.: Ocean pCO_2 calculated from dissolved inorganic carbon,
663   alkalinity, and equations for K1 and K2: validation based on laboratory measurements of CO2 in gas and
664   seawater at equilibrium, Mar. Chem., 70, 105-119, https://doi.org/10.1016/S0304-4203(00)00022-0, 2000.

665 Lüger, H., Wallace, D. W., Körtzinger, A., & Nojiri, Y.. The pCO2 variability in the midlatitude North Atlantic
666   Ocean during a full annual cycle. Global biogeochemical cycles, 18(3), 2004.

667 Martellucci, R., Salon, S., Cossarini, G., Piermattei, V., and Marcelli, M.: Coastal phytoplankton bloom dynamics
668   in the Tyrrhenian Sea: Advantage of integrating *in situ* observations, large-scale analysis and forecast systems,
669   J. Marine Syst., 218, 103528, https://doi.org/10.1016/j.jmarsys.2021.103528, 2021.

670 Mauri, E., Gerin, R., and Poulain, P.-M.: Measurements of water-mass properties with a glider in the South-western
671   Adriatic Sea, J. Oper. Oceanogr., 9, sup1, s3-s9, https://doi.org/10.1080/1755876X.2015.1117766, 2016.

672 Menna, M., Gačić, M., Martellucci, R., Notarstefano, G., Fedele, G., Mauri, E., Gerin, R., and Poulain, P. M.
673   Climatic, decadal, and interannual variability in the upper layer of the Mediterranean Sea using remotely sensed
674   and in-situ data. Remote Sensing, 14(6), 1322, 2022.

675 Menna, M., Martellucci, R., Reale, M., Cossarini, G., Salon, S., Notarstefano, G., Mauri, E., Poulain, P.-M., Gallo,
676   A., and Solidoro, C.: Impacts of an extreme weather system on the oceanographic features of the Mediterranean
677   Sea: the Medicane Apollo, Sci. Rep-UK, 13, 3870, https://doi.org/10.1038/s41598-023-29942-w, 2023.

678 Merchant, C. J., Embury, O., Bulgin, C. E., Block, T., Corlett, G. K., Fiedler, E., Good, S.A., Mittaz, J., Rayner,
679   N.A., Berry, D., Eastwood, S., Taylor, M., Tsushima, Y., Waterfall, A., Wilson R., Donlon, C.. Satellite-based
680   time-series of sea-surface temperature since 1981 for climate applications. *Scientific data*, *6*(1), 223. 2019.

681 Merlivat, L., and Brault, P.: CARIOCA Buoy: Carbon Dioxide Monitor, Sea Technol., 23–30, 1995.

682 Merlivat, L., Boutin, J., Antoine, D., Beaumont, L., Golbol, M., and Vellucci, V.: Increase of dissolved inorganic
683   carbon and decrease in pH in near-surface waters in the Mediterranean Sea during the past two decades,
684   Biogeosciences, 15, 5653–5662, https://doi.org/10.5194/bg-15-5653-2018, 2018.

685 Mihanović, H., Vilibić, I., Šepić, J., Matić, F., Ljubešić, Z., Mauri, E., Gerin, R., Notarstefano, G., and Poulain,
686   P.-M.: Observation, Preconditioning and Recurrence of Exceptionally High Salinities in the Adriatic Sea,
687   Front. Mar. Sci. 8, 834. https://doi.org/10.3389/fmars.2021.672210, 2021.

688 Millero F. J.. 2007 The Marine Inorganic Carbon Cycle. Chem Rev. 107(2):308-41. doi: 10.1021/cr0503557.

689 Neri, F., Romagnoli, T., Accoroni, S., Ubaldi, M., Garzia, A., Pizzuti, A., Campanelli, A., Grilli, F., Marini, M.,
690   and Totti, C.: Phytoplankton communities in a coastal and offshore stations of the northern Adriatic Sea
691   approached by network analysis and different statistical descriptors, Estuarine, Coastal and Shelf Science, 282,
692   108224, 2023.

693 Orr, J. C., Epitalon, J.-M., Dickson, A. G., and Gattuso, J.-P.: Routine uncertainty propagation for the marine
694   carbon dioxide system, Mar. Chem., 207, 84-107, https://doi.org/10.1016/j.marchem.2018.10.006, 2018.

695 Pastor, F., Valiente, J. A., and Palau, J. L.: Sea surface temperature in the Mediterranean: Trends and spatial
696   patterns (1982–2016). Meteorology and climatology of the Mediterranean and Black Seas, 297-309, 2019.

697 Paulsen, M. et al.: Data from RV Meteor 30 November, 2019 [Dataset], https://fileshare.icos-
698   cp.eu/s/eyLp9m685QA8ME7, 2023.

699 Pelletier, G., Lewis, E., and Wallace, D.: CO2SYS.XLS: A calculator for the CO2 system in seawater for Microsoft
700   Excel/VBA, Wash. State Dept. of Ecology/Brookhaven Nat. Lab., Olympia, WA/Upton, NY, USA, 2007.

701 Perez, F. F. and Fraga, F.: Association constant of fluoride and hydrogen ions in seawater, Mar. Chem., 21, 161–
702   168, https://doi.org/10.1016/0304-4203(87)90036-3, 1987.

703 Pinardi, N.; Cessi, P.; Borile, F.; Wolfe, C. The Mediterranean Sea Overturning Circulation. J. Phys. Oceanogr.
704   2019, 49, 1699–1721. 2019.

705 Pirro, A., Mauri, E., Gerin, R., Martellucci, R., Zuppelli, P., and Poulain, P.-M.: New insights on the formation
706   and breaking mechanism of convective cyclonic cones in the South Adriatic Pit during winter 2018, J. Phys.
707   Oceanogr., 52, 2049–2068, https://doi.org/10.1175/JPO-D-21-0108.1, 2022.

708 Poulain, P.-M., Centurioni, L., Özgökmen, T., Tarry, D., Pascual, A., Ruiz, S., Mauri, E., Menna, M., Notarstefano,
709   G.: On the Structure and Kinematics of an Algerian Eddy in the Southwestern Mediterranean Sea. Remote
710   Sensing, 13(15):3039. https://doi.org/10.3390/rs13153039, 2021.

711 Pranić, P., Denamie, C., Janeković, I., and Vilibić, I.: Multi-model analysis of the Adriatic dense-water dynamics,
712   Ocean Science, 19(3), 649-670, 2023.

713 Ravaioli, M., Bergami, C., Riminucci, F., Langone, L., Cardin, V., Di Sarra, A., Aracri, S., Bastianini, M., Bensi,
714   M., Bergamasco, A., Bommarito, C., Borghini, M., Bortoluzzi, G., Bozzano, R., Cantoni, C., Chiggiato, J.,
715   Crisafi, E., D'Adamo, R., Durante, S., Fanara, C., Grilli, F., Lipizer, M., Marini, M., Miserocchi, S., Paschini,
716   E., Penna, P., Pensieri, S., Pugnetti, A., Raicich, F., Schroeder, K., Siena, G., Specchiulli, A., Stanghellini, G.,
717   Vetrano, A., and Crise, A.: The RITMARE Italian Fixed-Point Observatory Network (IFON) for marine
718   environmental monitoring: a case study, J. Oper. Oceanogr., 9: sup1, s202-s214,
719   https://doi.org/10.1080/1755876X.2015.1114806, 2016.

720 Reverdin, G., Kestenare, E., Frankignoul, C., and Delcroix, T.: Surface salinity in the Atlantic Ocean (30 S–50 N).
721   Progress in Oceanography, *73*(3-4), 311-340, 2007.

722 Sabine, C., Sutton, A., McCabe, K., Lawrence-Slavas, N., Alin, S., Feely, R., ... & Tilbrook, B. (2020). Evaluation
723   of a new carbon dioxide system for autonomous surface vehicles. *Journal of Atmospheric and Oceanic
724   Technology*, *37*(8), 1305-1317.

725 Skjelvan, I., Coppola, L., Cardin, V., Juza, M., Bozzano, R., Pensieri, S., Giani, M., Siena, G., Urbini, L., Mauri,
726   E., Martellucci, R., Cantoni, C., Luchetta, A., Izquierdo, A., Paulsen, M., and Fiedler, B.: The ATL2MED
727   mission - experiences and lessons learnt, Technical report, ICOS-OTC, https://doi.org/10.18160/9HK5-807K,
728   2021.

729 Skjelvan, I., Fiedler, B., and Martellucci, R.: Data from Saildrone 1030 during the ATL2MED demonstration
730   experiment 2019-2020 [Data set], https://hdl.handle.net/11676/QN7XZKcJ2f4kBCGxQEeDdU3P, 2024a.

731 Skjelvan, I., Fiedler, B., and Martellucci, R.: Data from Saildrone 1053 during the ATL2MED demonstration
732   experiment 2019-2020 [Data set], https://hdl.handle.net/11676/9G9rntDvhmu-4nI4w91O11_g, 2024b.

733 Steinhoff, T., Gkritzalis, T., Lauvset S. K, Jones,S., Schuster, U., Olsen, A., Becker, M., Bozzano, R., Brunetti, F.,
734   Cantoni, C., Cardin, V., Diverrès, D., Fiedler, B., Fransson, A., Giani, M., Hartman, S., Hoppema, M.,
735   Jeansson, E., Johannessen, T., Kitidis, V., Körtzinger, A., Landa, C., Lefèvre, N., Luchetta, A., Naudts, L.,
736   Nightingale, P. D., Omar, A. M., Pensieri, S., Pfeil, B., Castaño-Primo, R., Rehder, G., Rutgersson, A., Sanders,
737   R., Schewe, I., Siena, G., Skjelvan, I., Soltwedel, T., van Heuven, S., and Watson, A.: Constraining the Oceanic
738   Uptake and Fluxes of Greenhouse Gases by Building an Ocean Network of Certified Stations: The Ocean
739   Component of the Integrated Carbon Observation System, ICOS-Oceans, Frontiers in Marine Science, vol. 6,
740   p. 544, doi:10.3389/fmars.2019.00544, 2019.

741 Sutton, A. J., Sabine, C. L., Maenner-Jones, S., Lawrence-Slavas, N., Meinig, C., Feely, R. A., Mathis, J. T.,
742   Musielewicz, S., Bott, R., McLain, P .D., Fought, J., and Kozyr, A.: A high-frequency atmospheric and
743   seawater pCO2 data set from 14 open ocean sites using a moored autonomous system, Earth Sys. Sci. Data, 6,
744   353–366, https://doi.org/10.5194/essd-6-353-2014, 2014.

745 Takahashi, T., Olafsson, J., Goddard, J. G., Chipman, D. W., and Sutherland, S. C.: Seasonal variation of CO_2 and
746   nutrients in the high-latitude surface oceans: a comparative study, Glob. Biogeochem. Cy., 7, 843-878,
747   https://doi.org/10.1029/93GB02263, 1993.

748 Takeshita, Y., Martz, T. R., Johnson, K. S., Plant, J. N., Gilbert, D., Riser, S. C., Craig. N. Tilbrook, B. (2013). A
749   climatology-based quality control procedure for profiling float oxygen data. Journal of Geophysical Research:
750   Oceans, 118(10), 5640-5650.

751 Tanhua, T., McCurdy, A., Fischer, A., Appeltans, W., Bax, N., Currie, K., DeYoung, B., Dunn, D., Heslop, E.,
752   Glover, L.K., Gunn, J., Hill, K., Ishii, M., Legler, D., Lindstrom, E., Miloslavich, P., Moltmann, T., Nolan, G.,

753 Palacz, A., Simmons, S., Sloyan, B., Smith, L.M., Smith, N., Telszewski, M., Visbeck, M., and Wilkin, J.:
754 What We Have Learned From the Framework for Ocean Observing: Evolution of the Global Ocean Observing
755 System. Front. Mar. Sci. 6:471. doi: 10.3389/fmars.2019.0047, 2019.
756 Testor, P., Mortier, L., Coppola, L., Claustre, H., D'Ortenzio, F., Bourrin, F., Durrieu de Madron, X., and
757 Raimbault, P., Glider MOOSE sections [data set], https://www.seanoe.org/data/00409/52027/, 2017.
758 Testor, P., de Young, B., Rudnick, D. L., Glenn, S., Hayes, D., Lee, C. M., Pattiaratchi, C., Hill, K., Heslop, E.,
759 Turpin, V., Alenius, P., Barrera, C., Barth, J. A., Beaird, N., Bécu, G., Bosse, A., Bourrin, F., Brearley, J. A.,
760 Chao, Y., Chen, S., Chiggiato, J., Coppola, L., Crout, R., Cummings, J., Curry, B., Curry, R., Davis, R., Desai,
761 K., DiMarco, S., Edwards, C., Fielding, S., Fer, I., Frajka-Williams, E., Gildor, H., Goni, G., Gutierrez, D.,
762 Haugan, P., Hebert, D., Heiderich, J., Henson, S., Heywood, K., Hogan, P., Houpert, L., Huh, S., Inall, E.,
763 Ishii, M., Ito, S.-i., Itoh, S., Jan, S., Kaiser, J., Karstensen, J., Kirkpatrick, B., Klymak, J., Kohut, J., Krahmann,
764 G., Krug, M., McClatchie, S., Marin, F., Mauri, E., Mehra, A., Meredith, P., Meunier, T., Miles, T., Morell, J.
765 M., Mortier, L., Nicholson, S., O'Callaghan, J., O'Conchubhair, D., Oke, P., Pallàs-Sanz, E., Palmer, M., Park,
766 J., Perivoliotis, L., Poulain, P.-M., Perry, R., Queste, B., Rainville, L., Rehm, E., Roughan, M., Rome, N.,
767 Ross, T., Ruiz, S., Saba, G., Schaeffer, A., Schönau, M., Schroeder, K., Shimizu, Y., Sloyan, B. M., Smeed,
768 D., Snowden, D., Song, Y., Swart, S., Tenreiro, M., Thompson, A., Tintore, J., Todd, R. E., Toro, C., Venables,
769 H., Wagawa, T., Waterman, S., Watlington, R. A., and Wilson, D.: OceanGliders: A component of the
770 integrated GOOS, Front. Mar. Sci., 6, https://doi.org/10.3389/fmars.2019.00422, 2019.
771 Ulses, C., Estournel, C., Fourrier, M., Coppola, L., Kessouri, F., Lefèvre, D., and Marsaleix, P.: Oxygen budget
772 of the north-western Mediterranean deep- convection region, Biogeosciences, 18, 937–960,
773 https://doi.org/10.5194/bg-18-937-2021, 2021.
774 Wong, A. P. S., Wijffels, S. E., Riser, S. C., Pouliquen, S., Hosoda, S., Roemmich, D., Gilson, J., Johnson, G. C.,
775 Martini, K., Murphy, D. J., Scanderbeg, M., Bhaskar, T. V. S. U., Buck, J. J. H., Merceur, F., Carval, T., Maze,
776 G., Cabanes, C., André, X., Poffa, N., Yashayaev, I., Barker, P. M., Guinehut, S., Belbéoch, M., Ignaszewski,
777 M., Baringer, M. O. N., Schmid, C., Lyman, J. M., McTaggart, K. E., Purkey, S. G., Zilberman, N., Alkire, M.
778 B., Swift, D., Owens, W. B., Jayne, S. R., Hersh, C., Robbins, P., West-Mack, D., Bahr, F., Yoshida, S., Sutton,
779 P. J. H., Cancouët, R., Coatanoan, C., Dobbler, D., Juan, A. G., Gourrion, J., Kolodziejczyk, N., Bernard, V.,
780 Bourlès, B., Claustre, H., D'Ortenzio, F., Le Reste, S., Le Traon, P. Y., Rannou, J. P., Saout-Grit, C., Speich,
781 S., Thierry, V., Verbrugge, N., Angel-Benavides, I. M., Klein, B., Notarstefano, G., Poulain, P. M., Vélez-
782 Belchí, P., Suga, T., Ando, K., Iwasaska, N., Kobayashi, T., Masuda, S., Oka, E., Sato, K., Nakamura, T., Sato,
783 K., Takatsuki, Y., Yoshida, T., Cowley, R., Lovell, J. L., Oke, P. R., van Wijk, E. M., Carse, F., Donnelly, M.,
784 Gould, W. J., Gowers, K., King, B. A., Loch, S. G., Mowat, M., Turton, J., Rama Rao, E. P., Ravichandran,
785 M., Freeland, H. J., Gaboury, I., Gilbert, D., Greenan, B. J. W., Ouellet, M., Ross, T., Tran, A., Dong, M., Liu,
786 Z., Xu, J., Kang, K. R., Jo, H. J., Kim, S. D., and Park, H. M.: Argo Data 1999–2019: Two Million
787 Temperature-Salinity Profiles and Subsurface Velocity Observations From a Global Array of Profiling Floats,
788 Front. Mar. Sci., 7, 700, https://doi.org/10.3389/fmars.2020.00700, 2020.
789 Zeebe R. E. Wolf-Gladrow D. 2007 CO2 in seawater: equilibrium, kinetics, isotope. Elsevier Matserdam, 346 pp.

790
791
792
793

Supplementary material

Table S1. Harbours and dates of SD maintenance, of which all took place in 2020.

Place / Drone	Mindelo (CV)	Telde, Gran Canaria (ES)	Porquerolles (FR)	Imperia (IT)	Cefalù, Sicily (IT)
SD 1030		12 February	22-23 April		26 May - 6 June
SD 1053	4-14 January			7 May	26 May - 6 June

797
798 **Table S2. Instruments, sensors, accuracy, and associated measurement frequency at the different fixed ocean stations,**
799 **gliders, and ship during the ATL2MED demonstration experiment.**

Instrument/ sensor	Company/ reference	Variable	Accuracy	Measurement frequency	Used by
SBE37	Sea-Bird Scientific	T Cond	0.002°C, 0.0003 S/m	10/min	DYFAMED
SBE41 (GPCTD)	Sea-Bird Scientific	T Cond	0.002°C, 0.0003 S/m	1/s	Glider MOOSE T00
SBE19	Sea-Bird Scientific.	T Cond	0.005°C, 0.0005 S/m	2/day	MIRAMARE
SBE16 plus v2	Sea-Bird Scientific	T Cond	0.005°C, 0.0005 S/m	12/day	W1M3A
SBE41 (GPCTD)	Sea-Bird Scientific	T Cond	0.002°C, 0.0003 S/m	1/s	Glider South Adriatic
SBE37-SMP-ODO	Sea-Bird Scientific	T Cond O_2	0.002°C, 0.0003 S/m, 3 µmol/kg	15/min 60/min	PALOMA, MIRAMARE
CARIOCA	Merlivat and Brault (1995)	pCO_2	2 µatm	24/day	DYFAMED
CO_2-proCV	Pro-Oceanus Systems Inc	pCO_2	2 µatm	12/day 6/day 24/day	W1M3A E2M3A MIRAMARE
Contros Hydro C systems	4H-JENA engineering GmbH	pCO_2	2 µatm	1/min	PALOMA
SBE21	Sea-Bird Scientific	Cond	0.001 S/m	2/min	RV Ucadiz

800 T= temperature; Cond=conductivity; O_2=dissolved oxygen; pCO_2=partial pressure of carbon dioxide.
801
802 **Table S3. Instruments and sensors at the SDs from Saildrone Inc. during the ATL2MED demonstration experiment**
803 **and used in this work.**

Instrument/ sensor	Company/ reference	Variable	Accuracy	Measurement frequency
SBE37-SMP-ODO (SD 1030; SD 1053)	Sea-Bird Scientific	T Cond O_2	0.002°C, 0.0003 S/m, 3 µmol/kg	10/min
ASVCO2 (SD 1030)	PMEL, Sutton et al. (2014)	pCO_2	2 µatm	24/day

804 T= temperature; Cond=conductivity; O_2=dissolved oxygen; pCO_2=partial pressure of carbon dioxide.

805
806 **Table S4. Instruments and methods used to analyse discrete samples collected at the RV Meteor and from different**
807 **fixed stations during the ATL2MED demonstration experiment.**

Instrument/ sensor	Company/ reference (SOP)	Variable	Accuracy	# measurements (depth)	Facility
Simultaneous potentiometric acid titration using a closed cell	SNAPO-CO2 prototype, Edmond (1970), Dickson and Goyet (1994)	DIC, TA	± 2 to 5 µmol/kg	1 (5 m)	DYFAMED

SOMMA	UiC (SOP 2), Johnson (1993)	DIC	2 µmol/kg	1 (5 m)	GEOMAR
VINDTA 3S/VINDTA 3C	MARIANDA (SOP 3b)	TA	3 µmol/kg	1 (5 m)	GEOMAR
Automatic potentiometric titrator	Hanna Instruments Titrator HI931	TA	± 4 µmol/kg	3 (6 m)	W1M3A
Automatic potentiometric titrator	Metrohm 685 Dosimat (Hernandez-Aylon, 1999)	TA	3 µmol/kg	5 (0.5, 3 m)[1]	PALOMA
Automatic potentiometric titrator	Mettler Toledo G20/SOP3b	TA	± 4 µmol/kg	10 (0.5, 2 m)	MIRAMARE
pH metre	Mettler Toledo Seven Compact	pH	± 0.001	3 (6 m)	W1M3A
Varian Cary 50 spectrophotometer	Varian, Clayton and Byrne (1993) (SOP 6b)	pH	± 0.003	5 (0.5, 3 m)[2]	PALOMA
Varian Cary 100 Spectrophotometer	Varian, Clayton and Byrne (1993) (SOP 6b)	pH	± 0.002	10 (0.5, 2 m)	MIRAMARE

808   O_2=dissolved oxygen; DIC=Dissolved Inorganic Carbon; TA=Total Alkalinity.
809   [1] For each measurement, 2 replicate samples were collected and analysed.
810   [2] For each measurement, 2 replicate samples were collected and 2-3 analyses were performed at each replicate.
811   SOP=Standard Operating Procedure according to Dickson et al. (2007).
812

813   **Table S5. Temperature offsets between SD sensor (SBE37-SMP-ODO) at 0.5 m depth and fixed stations during the**
814   **ATL2MED demonstration experiment. More details are available in Skjelvan et al. (2021).**

Fixed station/ glider	Measurement depth (m)	SD 1030 offset (°C)	SD 1053 offset (°C)
W1M3A	1	-0.006	-0.026
E2M3A	1.7	0.216	0.138
OGS ocean glider	0.5	0.063	0.063
PALOMA	0.5	0.077	0.090
PALOMA	3	-0.061	-0.046
MIRAMARE	0.5	-0.085	-0.205
MIRAMARE	2	-0.117	-0.238

815
816

817   **Table S6. Overview over where to find the data used in the current work.**

Platform	Variables used in current work	doi or pid	Reference
SD 1030	T, S, O_2, pCO_2	https://hdl.handle.net/11676/QN7XZKcJ2f4kBCGxQEeDdU3P	Skjelvan et al.(2024a)
SD 1053	T, S, O_2	https://hdl.handle.net/11676/9G9rntDvhmu-4nI4w91O11_g,	Skjelvan et al. (2024b)
RV Meteor	T, S, DIC, TA	https://fileshare.icos-cp.eu/s/eyLp9m685QA8ME7	Paulsen et al. (2023)

RV Ucadiz	S	https://fileshare.icos-cp.eu/s/eyLp9m685QA8ME7	Gonzalez and Bruno (2024)
DYFAMED/ BOUSSOLE fixed station	T, S, DIC, TA, pCO$_2$	https://doi.org/10.17882/43749	Coppola et al., 2023
Nice - Calvi glider	S	https://www.seanoe.org/data/00409/52027/, doi from the MOOSE program (glider SLOCUM Theque on MOOSE T00_43 section)	Testor et al. (2017)
W1M3A fixed station	T, S, pCO$_2$	https://hdl.handle.net/11676/Z9bGSnVObyglR0o8zcvmIXBz	Bozzano and Pensieri (2024)
E2M3A fixed station	T, S, pCO$_2$	https://nodc.ogs.it/catalogs/doidetails?4&doi=10.6092/d0d50095-bd30-4ff7-8d0a-a12121e72f78	Cardin et al. (2020)
E2M3A glider	S	https://nodc.ogs.it/catalogs/doidetails?8&doi=10.13120/e7277c6b-444a-4d61-8288-596af1bac3ff	Gerin et al. (2021)
PALOMA fixed station	T, S, pH, TA, pCO$_2$	https://hdl.handle.net/11676/an-PJSKTiEVHj3H0gA8ak3lG	Cantoni and Luchetta (2024)
MIRAMARE fixed station	T, S, pH, TA, pCO$_2$	https://hdl.handle.net/11676/ngPlu-Q0dtDcDx2wMFTNOtnZ	Giani (2024)
Argo buoy	S	https://doi.org/10.48670/moi-00044	Wong et al. (2020)
CMEMS	Model product	https://doi.org/10.25423/CMCC/MEDSEA_ANALYSISFORECAST_PHY_006_013_EAS7;	Clementi et al. (2021)
	Chl-a	OCEANCOLOUR_MED_BGC_L3_NRT_009_141, doi: 10.48670/moi-00297;	
	SST	SST_MED_SST_L4_NRT_OBSERVATIONS_010_004, doi:10.48670/moi-00172;	
	Vertical structure of sea temperature	MEDSEA_MULTIYEAR_PHY_006_004, doi:10.25423/CMCC/MEDSEA_MULTIYEAR_PHY_006_004_E3R	

818 T=temperature; S=salinity; O$_2$=dissolved oxygen; DIC=Dissolved Inorganic Carbon; TA=Total Alkalinity; pCO$_2$=partial
819 pressure of carbon dioxide.
820
821
822